Chemie der Erde 78 (2018) 521–534

Contents lists available at ScienceDirect

Chemie der Erde

journal homepage: www.elsevier.com/locate/chemer

Petrogenesis of plio-quaternary intra-plate continental alkaline lavas from the İskenderun Gulf (Southern Turkey): Evidence for metasomatized lithospheric mantle

Aykut Güçtekin

Department of Geology, University of Kocaeli, 41380 İzmit, Turkey

ARTICLE INFO

Handling Editor: T. Tomas Magna

Keywords:
Amphibole-peridotite melting
Intraplate volcanism
İskenderun Gulf
Metasomatic veins
Sr-Nd-Pb isotopes

ABSTRACT

The Quaternary alkaline volcanic field of Southern Turkey is characterized by intra-continental plate-type magmatic products, exposed to the north of the İskenderun Gulf along a NE-SW trending East Anatolian Fault, to the west of its intersection with the N–S trending Dead Sea Fault zone. The İskenderun Gulf alkaline rocks are mostly silica-undersaturated with normative nepheline and olivine and are mostly classified as basanites and alkaline basalts with their low-silica contents ranging between 43 and 48 wt.% SiO_2. They display Ocean Island Basalt (OIB)–type trace element patterns characterized by enrichments in large-ion-lithophile elements (LILE) and light rare earth element (LREE), and have $(La/Yb)_N$ = 8.8–17.7 and $(Hf/Sm)_N$ = 0.9–1.6 similar to those of basaltic rocks found in intraplate suites. The basanitic rocks have limited variations Sr-Nd isotopic ratios ($^{87}Sr/^{86}Sr$ = 0.70307–0.70324, $^{143}Nd/^{144}Nd$ = 0.512918–0.521947), whereas the alkali basalts display more evolved Sr-Nd isotopic ratios ($^{87}Sr/^{86}Sr$ = 0.70346-0.70365, $^{143}Nd/^{144}Nd$ = 0.512887–0.521896). The İskenderun Gulf alkaline rocks also display limited Pb isotopic variations with $^{206}Pb/^{204}Pb$ = 18.75–19.09 $^{207}Pb/^{204}Pb$ = 15.61–15.66 and$^{208}Pb/^{204}Pb$ = 38.65–39.02, indicating that they originated from an enriched lithospheric mantle source. Calculated fractionation vectors indicate that clinopyroxene and olivine are the main fractionating mineral phases. Similarly, based on Sr-Nd isotopic ratios, the assimilation and fractional crystallization (AFC) modeling shows that the alkali basalts were affected by AFC processes (r = 0.2) and were slightly contaminated by the upper crustal material.

The high TiO_2 contents, enrichments in Ba and Nb, and depletions in Rb can likely be explained by the existence of amphibole in the mantle source, which might, in turn, indicate that the source mantle has been affected by metasomatic processes. The modeling based on relative abundances of trace elements suggests involvement of amphibole-bearing peridotite as the source material. İskenderun Gulf alkaline rocks can thus be interpreted as the products of variable extent of mixing between melts from both amphibole-bearing peridotite and dry peridotite.

1. Introduction

Although effusive, low-volume ocean islandbasalt-type volcanism on continent is widespread worldwide, its origin and source region are still controversial. The studies carried out in some volcanic areas with low or no continental contamination may provide information about mantle composition of OIB-type magmas. It can be said that these magmas display large compositional variations, which indicates that they are the products of melt generation from a number of compositionally different mantle reservoirs, mixing between them at various proportions and variable melting degrees (e.g. Aldanmaz et al., 2006).

The magmas of intra-continental OIB type volcanism may be derived from hydrous sub-continental lithospheric mantle (SCLM; e.g. Hawkesworth and Gallagher, 1993) or from the asthenospheric mantle with slight contributions from SCLM (e.g. McKenzie and Bickle, 1988; White and McKenzie, 1989). When evaluating the contribution of the lithospheric mantle, care must be taken that the nature and composition of the lithospheric mantle are quite variable and sometimes cannot be easily distinguished from deep mantle sources. Lithospheric extensions, transtensional decompression or asthenospheric plumes may cause intra-continental alkaline volcanism (Turcotte and Emerman, 1983; White and McKenzie, 1989; Wilson and Downes, 1991). In such environments, the metasomatized, heterogeneous lithospheric mantle with enriched incompatible elements and low solidus temperatures is proposed to play a significant role for melt generation (Foley, 1992).

The re-fertilization of the mantle with low-degree metasomatic

E-mail address: a_guctekin@yahoo.com.

https://doi.org/10.1016/j.chemer.2018.08.001
Received 25 March 2018; Received in revised form 31 July 2018; Accepted 1 August 2018

melts is a mechanism for elucidating elevated abundances of incompatible trace elements and diagnostic isotope compositions of primitive alkaline rocks. Mantle metasomatism related compositional variations can be determined from mantle xenoliths gathered from the sub-continental lithospheric mantle (e.g. Kempton et al., 1988; O'Reilly et al., 1991; Ackerman et al., 2013). According to geochemical and isotopic studies, the trace element and isotope concentrations of OIB can be reflected by mixing of various mantle components such as fertile mantle, recycled oceanic lithosphere, or recycled sub-continental lithospheric mantle (e.g. Hofmann and White, 1982; White, 1985; Hart, 1988; Hart et al., 1992). Additionally, recycled oceanic crust preserved as eclogite, pyroxenite or amphibolite can constitute a part of the lithospheric mantle (Sobolev et al., 2005, 2007). The presence of such components in the mantle and their involvement in subsequent melt production result in variable trace element and isotope compositions.

Alkaline rocks of the İskenderun Gulf, which are the product of intra-continental volcanism in southern Turkey, are exposed through the Eastern Mediterranean Region (Fig. 1). These mafic volcanic rocks in the region are alkaline basalts and basanites with OIB character (Polat et al., 1997; Parlak et al., 1997; Yurtmen et al., 2000).The origin of these continental volcanic rocks with OIB-like geochemical signatures have previously been attributed to the lithospheric thinning caused by strike-slip faults and the partial melting due to decompression of the metasomatized asthenosphere (Polat et al., 1997; Bağcı et al., 2011).

Basaltic magmas erupted in intra-plate settings are commonly subjected to low-pressure fractional crystallization at different degrees. Fractionation strongly affects the bulk-rock composition and therefore only primitive rocks can be used for interpretation of characteristics of magma sources (Aldanmaz, 2002). In this study, the geochemical characteristics and modal mineralogy of the mantle source will be determined by using whole rock major and trace elements concentrations, and Sr, Nd and Pb isotope data of İskenderun Gulf intra-continental alkaline rocks. In addition to this, the possible effects, such as fractional crystallization and crustal contamination of mantle-derived magma and the melting processes forming alkaline magma will be examined.

2. Regional geology and characteristics of volcanic rocks

The İskenderun Gulf in the Eastern Mediterranean Region is located between the African and Arabian plates, and the Anatolian collision zone (Fig. 1). Since the Early Pliocene the plate movements in the Eastern Mediterranean formed a triple joint known as "Maras Triple Junction" in Kahramanmaraş, where the Dead Sea Fault, the Eastern Anatolian Fault and the northeast extension of the Cyprus Arch intersect (Fig. 1a, b; Şengör and Yılmaz, 1981; Karig and Kozlu, 1990; Kozlu, 1987; Fyitkas et al., 1984). The movements of the Arabian and African plates towards the Anatolian plate formed the fault zones and deformations in the region (McKenzie, 1972; Şengör and Yılmaz, 1981; Fyitkas et al., 1984; İzzeldin, 1987; Bayer et al., 1988; Le Pichon and Gaulier, 1988; Yılmaz et al., 1988; Yürür and Chorowıcz, 1998; Albora et al., 2006).

The İskenderun Gulf area is located between the Misis Range in the north and the Amanos Range in the east (Fig. 1a). The Misis Range is an olistostromic complex tectonically emplaced onto Miocene to Early Pliocene marine sediments (Kelling et al., 1987). The Amanos Range in the east is the fragment of the continental crust, which is separated from the Arabian Platform by the NE-SW left-lateral Karatas-Osmaniye Fault Zone (KFZ) and usually included in the African plate (Adıyaman and Chorowicz, 2002).

The Plio-Quaternary intra-continental volcanic rocks in the İskenderun Gulf area (Arger et al., 2000), outcrop along the northeast-southwest KFZ (Fig. 1a; KOFZ; Şaroğlu et al., 1992). Deli Halil Hill, Üçtepeler, Toprakkale, Gertepe, and some smaller morphologically preserved cinder cones represent eruptive centers of the studied basaltic lavas. Dali Halil Hill represents a small, but rather complex volcano, with a central cone, several parasitic craters and lava flows. The cone is built of basaltic scoria (Yurtmen et al., 2000). Olivine phenocrysts and ellipsoidal vesicles are apparent in basaltic lava with blocky surface (aa-type). Columnar jointing with thin columns (40–50 cm) can be seen where inner section of the lava is exposed. The cones consist of alternating layers of black and red (oxidized) scoriae with clast-supported structure, suggesting fall deposition. The scorias contain lava shreds and bombs (up to 30 cm). The character of deposits implies a Strombolian style eruption (Walker, 1973; Cas and Wright, 1987). The scoria cones of Gertepe and Üçtepeler located to the north of Deli Halil Hill are elongated approximately E-W. The lava flows are intercalated with alluvial fan deposits of Quaternary age (Yurtmen et al., 2000). The ages of the volcanic rocks containing alkali olivine basalt and basanitic rocks were determined to be younger than 2.25 Ma according to bulk-rock K-Ar ages (Arger et al., 2000).

3. Petrography

Petrography of the alkali basalts and basanites from the İskenderun Gulf was described by Yurtmen et al. (2000) and Bağcı et al. (2011). The majority of alkali basalts have intergranular, interstitial texture and some of them have a vesicular structure. The phenocryst size is about 1.5 mm and proportion of phenocrysts to matrix varies between 15 and 25%. Olivines are euhedral and subhedral, mostly not altered, but occasionally iddingsitized along margins. Skeletal and embayment textures are also found in some olivine phenocrysts. Clinopyroxene in the form of microphenocrysts is subhedral to euhedral. Plagioclase, olivine, clinopyroxene and opaque minerals constitute the matrix.

Basanites display interstitial, pilotaxitic and weakly porphyric textures, with common euhedral and subhedral olivine phenocrysts. The phenocryst size is about 2 mm and the proportion of phenocrysts to matrix is < 10%. There are also melt inclusions in the olivines, where skeleton and embayment textures are observed. Some olivines are fractured and iddingsitized along the crystal margins and fractures. The matrix is composed of plagioclase, olivine, clinopyroxene, nepheline and opaque minerals. The opaque minerals in these series were defined as titanomagnetite by Yurtmen et al. (2000).

4. Analytical techniques

Twenty-five alkaline volcanic rocks from the İskenderun Gulf were sampled for major and trace-element analyses. Major and trace element concentrations were determined by inductively coupled plasma emission spectrometry (ICP-AES) and inductively coupled plasma mass spectrometry (ICP-MS) at Analytical Laboratories (ACME, Canada). Analyses of major and trace elements were made with the 4 A + 4B package method. 0.2 g of rock-powder was fused with 1.5 g $LiBO_2$ and then dissolved in 100 ml 5% HNO_3. The loss on ignition (LOI) values were obtained by heating the dried samples at 1000 °C. The detection limits range from 0.01 to 0.1 wt.%, for major oxides, 0.1 to 10 ppm for trace elements and 0.01 to 0.5 ppm for the rare earth elements. The major and trace element contents and the sample locations are given in Table 1.

For Sr-Nd isotope analysis, 9 samples were selected from alkali basalt and basanitic rocks based on geochemical characteristics. Sr-Nd isotopic analyses were performed at the Middle East Technical University (Radiogenic Isotope Laboratory) Ankara, Turkey, using analytical techniques described in Romer et al. (2001). Isotope ratios were measured using TIMS (Triton Multi-Collector Thermal Ionization Mass Spectrometer) and analytical uncertainties were given at 2 sigma levels. Ratios of $^{87}Sr/^{86}Sr$ are normalized to $^{86}Sr/^{88}Sr = 0.1194$ (Nier, 1938), and $^{143}Nd/^{144}Nd$ data are normalized to $^{143}Nd/^{144}Nd = 0.7219$ (O'Nions et al., 1979). During the course of the measurement, NBS 987 and Nd LaJolla international standards were measured with $^{87}Sr/^{86}Sr$ and $^{143}Nd/^{144}Nd$ of 0.710244 ± 8 (n = 3) and 0.511852 ± 2 (n = 2), respectively. The USGS reference material BCR-1 gave $^{87}Sr/^{86}Sr = 0.705014 \pm 5$ and $^{143}Nd/^{144}Nd = 0.512638 \pm 4$.

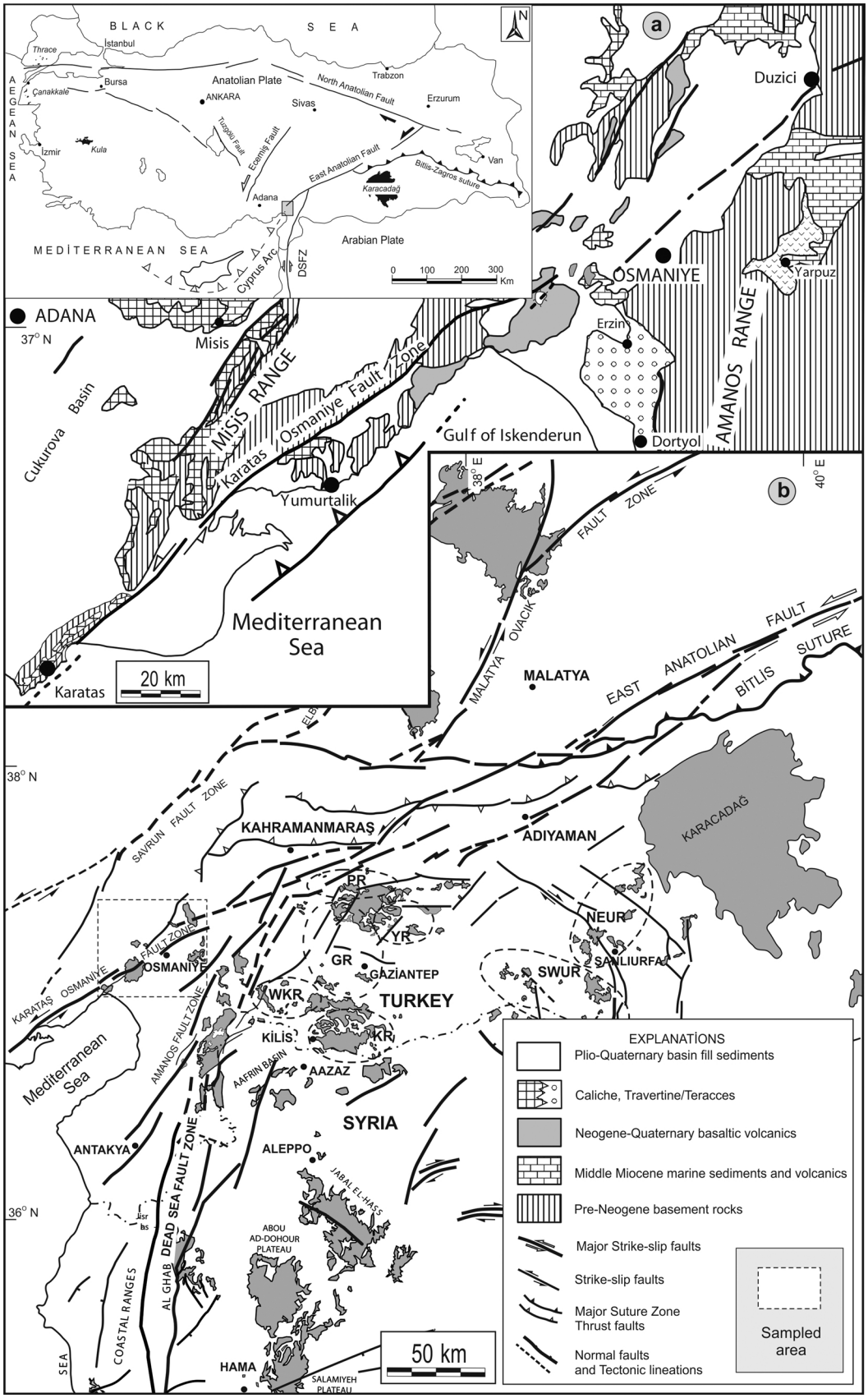

Fig. 1. (a) Geological map of the İskenderun Gulf and its surroundings showing major faults and volcanic outcrops, modified from Gürsoy et al., 2003 (based on the 1:100,000 geological map of Turkey). Inset figure show the alkaline volcanic suits (black areas) of Kula, Çanakkale, Thrace and Karacadağ, respectively. (b) Simplified map of southern Turkey and northwestern Syria highlighting the distribution of Cenozoic volcanic rocks (Gürsoy et al., 2009; Ma et al., 2013). Abbreviations: GR: Gaziantep Region; KR: Kilis Region; PR: Pazarcık Region; YR: Yavuzeli Region; WKR: Western Kilis Region; SWUR: SW Urfa Region; NEUR: NE Urfa Region.

Table 1
Whole-rock major and trace element data for the representative samples from İskenderun Gulf alkaline volcanic rocks.

Sample No	O-1	O-2	O-3	O-4	O-5	O-6	O-7	O-9	O-10	O-11	O-12	O-14	
Rock Type	Basanite	Basanite	Basanite	Basanite	Al. Bas.	Basanite	Al. Bas.	Al. Bas.	Al. Bas.	Al. Bas.	Al. Bas.	Al. Bas.	
Longitude	36° 04′ 16″ E	36° 04′ 15″ E	36° 05′ 14″ E	36° 05′ 16″ E	36° 08′ 06″ E	36° 08′ 09″ E	36° 08′ 08″ E	36° 08′ 24″ E	36° 07′ 55″ E	36° 07′ 59″ E	36° 08′ 01″ E	36° 03′ 19″ E	
Latitude	37° 02′ 09″ N	37° 02′ 10″ N	37° 02′ 15″ N	37° 02′ 10″ N	37° 03′ 06″ N	37° 03′ 04″ N	37° 02′ 28″ N	37° 01′ 37″ N	37° 01′ 41″ N	37° 01′ 53″ N	37° 01′ 56″ N	37° 06′ 32″ N	MDL
SiO_2	43.22	43.38	46.13	46.34	48.02	43.67	47.32	47.10	45.48	47.18	46.67	45.34	0.01
TiO_2	2.90	2.90	2.52	2.54	1.94	2.89	1.96	2.06	1.84	2.02	2.07	2.47	0.01
Al_2O_3	14.38	14.28	15.99	16.01	15.15	14.64	14.95	14.75	14.38	14.78	14.72	15.26	0.01
Fe_2O_3	13.27	13.17	11.15	11.38	12.46	13.18	12.77	12.98	12.45	12.80	12.78	12.17	0.01
MnO	0.18	0.18	0.18	0.19	0.16	0.18	0.15	0.17	0.17	0.17	0.17	0.16	0.01
MgO	9.65	9.49	7.17	7.30	7.92	9.29	7.42	8.58	8.80	8.56	8.72	8.79	0.01
CaO	9.46	9.29	7.58	7.64	9.70	10.26	9.72	9.79	11.14	9.81	9.79	10.12	0.01
Na_2O	4.18	3.71	5.19	4.98	3.19	3.59	2.96	3.36	3.03	3.27	3.08	3.26	0.01
K_2O	1.63	1.91	2.72	2.45	0.73	1.42	0.68	0.89	0.73	0.82	0.87	1.12	0.01
P_2O_5	0.98	1.04	0.71	0.72	0.33	0.86	0.32	0.38	0.32	0.36	0.40	0.42	0.01
L.O.I.	0.3	0.2	0.3	0.1	0.1	0.4	1.4	0.4	1.4	0.1	0.4	0.6	0.01
Total	99.61	99.62	99.67	99.68	99.76	99.65	99.73	99.74	99.75	99.74	99.73	99.71	
Sc	21	21	18	19	23	24	23	24	24	23	23	26	1
Cr	246.3	246.3	109.5	116.3	266.9	239.5	266.9	287.3	307.9	287.3	287.3	205.2	
V	208	203	163	166	193	235	203	204	195	203	203	236	8
Ni	195	189	114	117	112	164	120	152	151	146	151	135	20
Co	50.7	48.1	37.4	35.5	44.6	48.9	44.3	47.7	49.1	48.5	47.4	50.1	0.2
Cu	58.5	64.8	37.7	33.7	37.7	52.9	43.5	43.6	40.1	41.4	31.2	43.3	0.1
Zn	90	93	65	55	62	70	73	75	70	69	56	60	1
Ga	19.8	20.3	20.2	19.6	18.5	19.6	19.8	19.5	18.6	19.5	17.9	18.9	0.5
Rb	18.7	19.5	31.4	33.1	6.8	13.4	4.2	9.1	7.2	7.8	8.7	9.1	0.1
Sr	1046	1054	845.8	817.3	484.6	953.7	797.8	551.7	498.1	518.7	531.1	670.4	0.5
Y	22.3	23.0	24.7	24.3	18.2	22.2	18.3	18.4	16.1	17.7	17.7	19.5	0.1
Zr	219.5	221.9	324.5	315.5	107.1	169.4	103.5	117.9	102.2	113.2	119.8	138.2	0.1
Nb	58.0	58.1	60.9	60.7	16.0	42.2	15.6	19.8	16.1	18.9	20.2	24.6	0.1
Ba	358	355	346	324	166	309	171	195	153	169	196	201	1
La	40.3	42.6	44.3	43.8	19.1	34.7	18.9	20.8	17.4	19.1	20.7	21.8	0.1
Ce	84.8	86.0	83.6	83.3	37.3	69.5	36.1	42.4	34.6	39.4	41.8	44.8	0.1
Pr	10.10	10.33	9.44	9.27	4.53	8.67	4.42	4.99	4.14	4.69	4.92	5.33	0.02
Nd	40.5	43.5	37.1	33.5	18.0	35.8	19.6	20.8	17.0	19.7	21.5	22.3	0.3
Sm	7.70	8.04	6.78	6.58	4.00	6.88	4.10	4.53	3.69	4.24	4.42	4.90	0.05
Eu	2.55	2.61	2.17	2.17	1.45	2.32	1.48	1.58	1.36	1.56	1.56	1.67	0.02
Gd	6.71	6.93	5.90	6.12	4.25	6.11	4.39	4.47	4.14	4.53	4.47	4.63	0.05
Tb	0.97	0.99	0.90	0.93	0.69	0.95	0.68	0.72	0.64	0.69	0.71	0.75	0.01
Dy	4.91	5.17	5.03	4.93	3.70	4.97	3.86	3.95	3.47	3.81	3.98	3.97	0.05
Ho	0.82	0.85	0.94	0.92	0.69	0.89	0.70	0.70	0.63	0.68	0.69	0.74	0.02
Er	2.13	2.21	2.57	2.48	1.76	2.19	1.85	1.91	1.76	1.86	1.79	2.03	0.03
Tm	0.27	0.29	0.35	0.34	0.24	0.30	0.26	0.25	0.23	0.24	0.26	0.27	0.01
Yb	1.63	1.70	2.35	2.21	1.54	1.74	1.58	1.60	1.41	1.47	1.56	1.62	0.05
Lu	0.24	0.24	0.35	0.32	0.23	0.25	0.22	0.23	0.20	0.23	0.22	0.23	0.01
Hf	5.5	5.5	7.4	6.8	2.8	4.2	3.4	2.9	3.0	3.2	3.2	3.4	0.1
Ta	3.4	3.8	4.1	4.4	1.0	2.5	1.0	1.2	1.0	1.1	1.1	1.4	0.1
Pb	2.3	2.9	1.2	1.2	1.2	1.3	1.7	1.5	1.3	1.3	1.1	1.3	0.1
Th	3.9	4.2	7.6	8.1	2.6	3.0	2.0	2.3	2.2	2.4	2.2	1.9	0.2
U	1.2	1.4	2.2	2.3	0.6	0.9	0.2	0.6	0.4	0.6	0.6	0.6	0.1
Mg#	61.6	61.3	58.6	58.8	58.3	60.0	56.1	59.3	60.9	59.6	60.0	61.4	
Fractionation corrected values													
Rb	14.80	15.43	22.97	23.89	4.91	10.34	2.82	6.75	5.55	5.86	6.62	7.20	
Sr	884.2	850.7	635.3	606.3	359.5	752.0	554.3	419.6	392.7	399.3	413.8	541.1	
K	10693	12530	16491	14650	4365	9080	3784	5469	4668	5107	5491	7347	
La	32.1	33.9	32.7	31.9	13.9	26.9	12.8	15.5	13.5	14.4	15.8	17.3	
Nb	45.8	45.9	44.4	43.7	11.5	32.5	10.4	14.6	12.4	14.1	15.3	19.4	
Dy	4.11	4.33	3.97	3.85	2.89	4.09	2.86	3.15	2.85	3.07	3.24	3.33	
Yb	1.35	1.41	1.83	1.71	1.19	1.41	1.15	1.26	1.14	1.17	1.25	1.34	
Th	3.1	3.3	5.6	5.8	1.8	2.3	1.3	1.7	1.7	1.8	1.6	1.5	

Sample No	O-16	O-17	O-18	O-19	O-21	O-22	O-23	O-24	O-26	O-27	O-28	O-30	O-31
Rock Type	Basanite	Basanite	Basanite	Basanite	Basanite	Basanite	Basanite	Basanite	Basanite	Al. Bas.	Basanite	Al. Bas.	Basanite
Longitude	36° 04′ 26″ E	36° 04′ 47″ E	36° 04′ 44″ E	36° 04′ 55″ E	36° 05′ 17″ E	36° 05′ 29″ E	36° 05′ 36″ E	36° 05′ 30″ E	36° 05′ 35″ E	36° 59′ 59″ E	36° 09′ 20″ E	36° 08′ 00″ E	36° 11′ 06″ E
Latitude	37° 06′ 52″ N	37° 06′ 58″ N	37° 06′ 56″ N	37° 06′ 50″ N	37° 07′ 01″ N	37° 06′ 55″ N	37° 07′ 15″ N	37° 02′ 14″ N	37° 02′ 20″ N	36° 05′ 42″ N	37° 04′ 10″ N	37° 01′ 47″ N	37° 06′ 30″ N
SiO_2	44.62	44.76	45.82	45.00	44.43	45.32	44.39	45.30	45.04	47.68	44.18	47.22	43.9
TiO_2	2.86	2.79	2.62	2.80	2.80	2.73	2.49	2.70	2.76	1.84	3.46	2.03	2.29
Al_2O_3	14.93	14.88	15.66	14.77	14.88	15.73	15.31	15.38	15.04	14.66	14.83	14.78	13.62
Fe_2O_3	11.37	11.74	11.13	11.66	11.90	11.20	10.72	11.49	11.51	12.61	12.67	12.84	12.79
MnO	0.17	0.17	0.17	0.17	0.17	0.17	0.16	0.17	0.17	0.17	0.17	0.17	0.17

(*continued on next page*)

Table 1 (*continued*)

Sample No	O-16	O-17	O-18	O-19	O-21	O-22	O-23	O-24	O-26	O-27	O-28	O-30	O-31
Rock Type	Basanite	Basanite	Basanite	Basanite	Basanite	Basanite	Basanite	Basanite	Basanite	Al. Bas.	Basanite	Al. Bas.	Basanite
Longitude	36° 04′ 26″ E	36° 04′ 47″ E	36° 04′ 44″ E	36° 04′ 55″ E	36° 05′ 17″ E	36° 05′ 29″ E	36° 05′ 36″ E	36° 05′ 30″ E	36° 05′ 35″ E	36° 59′ 59″ E	36° 09′ 20″ E	36° 08′ 00″ E	36° 11′ 06″ E
Latitude	37° 06′ 52″ N	37° 06′ 58″ N	37° 06′ 56″ N	37° 06′ 50″ N	37° 07′ 01″ N	37° 06′ 55″ N	37° 07′ 15″ N	37° 02′ 14″ N	37° 02′ 20″ N	36° 05′ 42″ N	37° 04′ 10″ N	37° 01′ 47″ N	37° 06′ 30″ N
MgO	9.02	9.31	7.67	9.09	9.38	8.08	8.03	8.62	9.04	8.56	6.26	8.07	12.28
CaO	8.50	8.51	7.31	8.57	8.67	7.83	7.38	8.03	8.50	9.73	11.42	9.82	8.57
Na_2O	4.57	4.49	5.05	4.49	4.40	4.97	4.64	4.84	4.34	3.29	3.47	3.16	3.69
K_2O	2.38	2.15	2.77	2.27	2.24	2.55	2.47	2.50	2.11	0.70	1.51	0.81	1.51
P_2O_5	0.73	0.76	0.72	0.78	0.78	0.73	0.63	0.74	0.76	0.41	0.89	0.36	0.86
L.O.I.	0.4	0.0	0.7	0.0	0.1	0.3	3.4	0.2	0.3	0.0	0.8	0.4	0.2
Total	99.64	99.64	99.66	99.64	99.63	99.66	99.67	99.65	99.65	99.72	99.67	99.73	99.60
Sc	21	21	18	21	21	19	18	20	21	22	25	23	20
Cr	212.1	225.8	136.9	232.6	225.8	164.2	198.41	184.7	218.9	342.1	102.6	287.3	335.2
V	236	231	187	222	217	198	174	202	204	200	263	216	192
Ni	160	177	130	178	184	138	148	159	175	176	54	139	322
Co	47.6	50.2	42.8	48.3	48.6	42.3	47.8	46.5	46.8	53.2	42.6	52.6	62.9
Cu	39.3	41.1	32.6	45.1	44.4	37.1	100.9	36.9	41.9	39.0	46.6	42.2	46.2
Zn	59	60	59	60	59	56	57	61	59	85	71	72	68
Ga	21.2	21.5	22.7	19.3	20.0	20.3	17.9	21.1	18.4	18.8	20.6	19.4	17.8
Rb	24.6	24.3	29.0	22.8	22.8	27.7	26.0	26.0	23.0	9.5	13.8	7.6	16.8
Sr	917.9	910.8	881.1	945.6	938.7	888.3	802.9	888.6	894.9	602.8	1060	550.4	907.3
Y	23.7	24.0	24.7	24.3	23.5	24.2	21.5	24.1	23.0	19.6	24.1	19.7	20.8
Zr	274.1	271.9	327.9	266.5	264.3	306.3	291.8	298.3	258.2	130.3	194.5	123.1	202.8
Nb	55.8	52.8	60.4	53.4	51.8	56.1	52.3	54.9	49.4	22.7	55.5	19.6	44.5
Ba	325	319	317	324	313	313	271	309	300	250	407	283	316
La	41.4	40.6	39.8	39.3	38.9	40.8	34.6	38.9	37.5	32.3	34.7	19.9	39.0
Ce	79.7	78.0	81.0	80.7	80.5	80.5	71.7	78.7	77.1	63.4	80.6	43.3	80.9
Pr	9.54	9.29	9.21	9.32	9.26	9.17	7.73	8.96	8.76	6.81	9.54	4.76	8.62
Nd	39.5	37.6	35.9	38.4	36.1	36.6	29.5	35.5	34.8	25.2	41.6	20.8	34.7
Sm	6.99	7.02	6.86	7.02	7.10	6.68	5.54	6.62	6.66	4.87	7.82	4.45	6.43
Eu	2.25	2.30	2.20	2.21	2.19	2.21	1.90	2.22	2.24	1.71	2.68	1.58	2.20
Gd	6.06	6.37	5.96	6.18	6.21	6.20	5.31	6.20	6.17	4.68	7.31	4.57	5.74
Tb	0.92	0.95	0.93	0.93	0.91	0.91	0.79	0.91	0.91	0.74	1.02	0.72	0.84
Dy	4.77	4.96	4.81	4.75	4.82	4.74	4.03	4.67	4.71	3.76	4.81	3.67	4.17
Ho	0.87	0.86	0.85	0.85	0.87	0.87	0.79	0.88	0.84	0.73	0.95	0.71	0.78
Er	2.26	2.38	2.51	2.39	2.29	2.36	2.03	2.37	2.26	1.92	2.27	1.83	1.98
Tm	0.33	0.34	0.35	0.32	0.33	0.35	0.32	0.33	0.32	0.27	0.29	0.26	0.28
Yb	1.94	1.96	2.13	1.87	1.89	2.18	1.83	2.17	1.93	1.66	1.85	1.62	1.65
Lu	0.29	0.29	0.31	0.28	0.28	0.30	0.26	0.29	0.27	0.24	0.25	0.22	0.22
Hf	5.6	5.9	7.0	6.0	6.0	6.2	6.3	7.1	5.8	3.2	4.9	2.8	4.1
Ta	3.6	3.5	3.9	3.1	3.3	3.5	3.3	3.5	3.3	1.4	3.0	1.0	2.6
Pb	2.2	1.0	2.4	1.8	1.0	1.7	1.8	1.1	1.0	0.8	1.4	1.6	1.1
Th	5.4	4.9	5.1	4.4	5.0	5.8	5.1	5.5	4.5	5.2	2.9	2.1	4.4
U	1.6	1.4	1.7	1.5	1.6	1.8	1.8	1.8	1.3	1.1	0.8	0.5	1.1
Mg#	63.6	63.6	60.3	63.2	63.4	61.3	62.2	62.3	63.3	59.9	52.1	58.0	67.9
Fractionation corrected values													
Rb	20.44	20.20	24.08	18.72	18.95	21.64	21.09	21.09	19.12	7.23	8.31	5.41	15.13
Sr	774.8	768.9	686.5	789.5	792.4	708.7	662.9	733.7	755.4	469.7	666.2	403.1	824.4
K	16403	14818	17483	15456	15438	16517	16614	16815	14542	4418	7526	4776	11283
La	34.6	33.9	30.5	32.4	32.5	32.1	28.2	31.7	31.3	24.8	21.2	14.3	35.2
Nb	46.3	43.8	45.9	43.8	43.0	43.7	42.3	44.4	41.0	17.2	33.3	13.9	40.0
Dy	4.15	4.31	3.92	4.09	4.19	3.93	3.44	3.99	4.09	3.06	3.28	2.84	3.85
Yb	1.67	1.64	1.71	1.60	1.63	1.79	1.55	1.84	1.66	1.33	1.24	1.24	1.51
Th	4.5	4.0	3.9	3.6	4.1	4.5	4.1	4.4	3.7	3.9	3.7	1.5	3.9

Pb isotope ratios were performed at the Laboratoire G-Time of the Université Libre de Bruxelles (Belgium). To remove alteration and any potential contamination, a leaching procedure was applied to powdered whole rock samples (250 mg), with repeated additions (5–6 times) of 6 N sub-boiled HCl followed by 30-minutes ultrasonic baths until the solution was clear. Lead separation was completed using successive acid elution on anionic resin column (e.g. Weis et al., 2006). Analytical uncertainties are given at 2-sigma level. Analyses of the SRM981 Pb standard solution yielded $^{208}Pb/^{204}Pb = 36.7174 \pm 47$, $^{207}Pb/^{204}Pb = 15.4978 \pm 13$, and $^{206}Pb/^{204}Pb = 16.9408 \pm 20$.

5. Results

5.1. Major and trace element characteristics

The mafic extrusive rocks are classified using the total alkali ($Na_2O + K_2O$) versus SiO_2 (TAS) in the diagram of Le Bas et al. (1986). According to this diagram, the rocks are all alkaline and classified as basanite and alkali basalt (Fig. 2). The rocks are silica-undersaturated, sodic ($Na_2O/K_2O = 1.82–4.70$) and have SiO_2 concentrations between 43 and 48%. The alkali basalts have moderate MgO (7–8 wt.%),

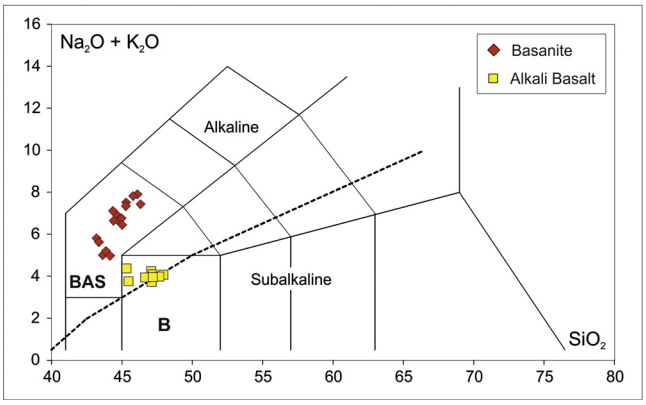

Fig. 2. Classification of the volcanic rocks from the İskenderun Gulf on a TAS diagram of Le Bas et al. (1986). Key to abbreviations: B: basalt; BAS: basanite.

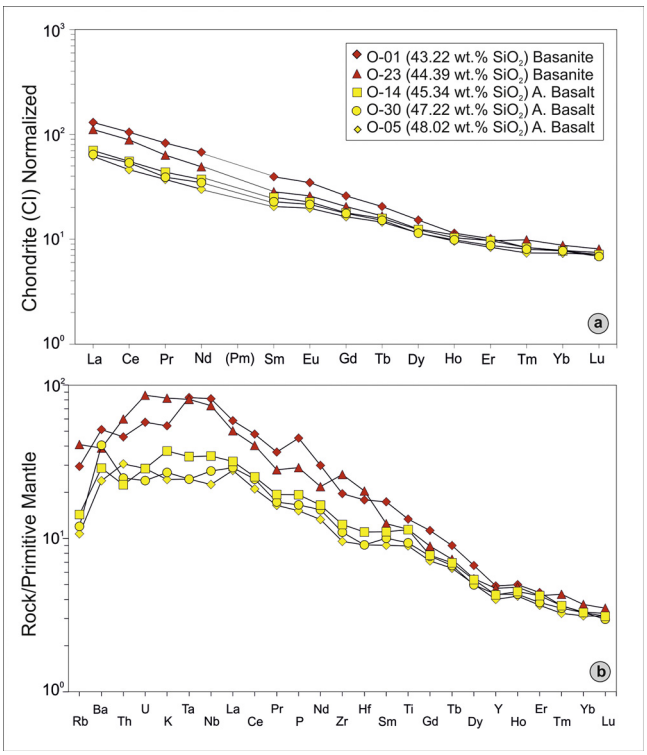

Fig. 3. (a) Chondrite-normalized REE element patterns for the İskenderun Gulf volcanic rocks. Chondrite normalising values are from Boynton (1984). (b) Primitive mantle normalized multielement patterns for the Gulf of Iskenderun volcanic rocks. Primitive mantle normalising values are from Sun and McDonough (1989).

whereas the basanites have a wide range of MgO contents (6–12 wt.%). Mg-number (Mg-number = 100Mg/(Mg/Fe)) varies from 58 to 60 for the alkali basalt samples and from 52 to 67 for the basanite samples. The rocks have high Al_2O_3 (14–16 wt.%) contents (Table 1). The CaO contents of the alkali basalt samples (9–11 wt.%) are generally higher than the basanite samples (7–11 wt.%). The Cr and Ni concentrations of the alkali basalts vary from 205 to 342 and from 112 to 176, respectively, while those of the basanite samples are between 102 and 335 ppm, and 54 and 322 ppm. In the chondrite-normalized (Boynton, 1984) REE diagram, the samples form a regular and semi-parallel patterns and there is common enrichment in LREE relative to HREE (Fig. 3a). The basanite samples are characterized by steeper REE patterns compared with alkaline basalts. The alkali basalts have $(La/Yb)_N$ ratios from 8 to 13 while $(La/Yb)_N$ = 13–17 in basanites. Primitive mantle normalized (Sun and McDonough, 1989) trace element diagrams for the İskenderun Gulf alkaline rocks is shown in Fig. 3b. On the primitive mantle-normalized multi-element diagrams, the basanite samples show positive Nb-Ta anomalies, with incompatible trace-element abundances higher than the alkali basalt samples.

5.2. Sr-Nd-Pb-isotopic systematics

The measured Sr, Nd and Pb isotopic ratios of volcanic rocks are given in Table 2. The Sr-Nd isotope ratios of alkaline basalts are more radiogenic than those of basanites. The $^{87}Sr/^{86}Sr$ isotope ratios of alkali basalts and basanites are 0.70346 - 0.70365 and 0.70307 - 0.70324, respectively. The $^{143}Nd/^{144}Nd$ isotope ratios are 0.512887 - 0.512896 in alkali basalts and 0.512918-0.512947 in basanites. For comparison, the diagrams include also the fields for MORB, OIB, CiMACI (the Circum-Mediterranean Anorogenic Cenozoic Igneous Province; Lustrino and Wilson, 2007) and several intra-plate lava suites, using data from a wider region (Fig. 4). In the $^{143}Nd/^{144}Nd$ vs $^{87}Sr/^{86}Sr$ correlation plot, İskenderun Gulf alkaline lavas in OIB area are similar to NW Anatolian alkaline lavas, Karacadağ lavas and some NW Syria samples and basanites showing depleted-like pattern and alkali basalts being more enriched-like. The samples plot in the PREMA quadrangle relative to Bulk Silicate Earth and show a clear negative correlation (Fig. 4a).

The Pb isotope compositions of the samples are: $^{206}Pb/^{204}Pb$ = 19.02–19.08, $^{207}Pb/^{204}Pb$ = 15.64–15.66, $^{208}Pb/^{204}Pb$ = 38.98–39.02 for alkali basalts and $^{206}Pb/^{204}Pb$ = 18.75–19.09, $^{207}Pb/^{204}Pb$ = 15.60–15.63, $^{208}Pb/^{204}Pb$ = 38.65–38.88 for basanites. In the $^{143}Nd/^{144}Nd$ vs. $^{206}Pb/^{204}Pb$ plot, all the samples fall in the OIB field and cluster between the Bulk Silicate Earth (BSE) and MORB fields (Fig. 4b). In the $^{207}Pb/^{204}Pb$ - ^{206}Pb / ^{204}Pb plot, the rocks fall on the right of geochron above the NHRL line ($\Delta^{7/4}$ up to 11.20; $\Delta^{8/4}$ up to 38.40; Table 2, Fig. 4c). There is a slight trend towards EMII in the alkali basalt samples. Similarly, in the $^{208}Pb/^{204}Pb$-$^{206}Pb/^{204}Pb$ diagram, the rocks are coherent to the above-mentioned OIB-type rocks, while alkali basalts form a trend towards the EMII composition (Fig. 4d). The alkali basalts are shifted towards a HIMU component in $^{143}Nd/^{144}Nd$-$^{208}Pb^*/^{206}Pb^*$ diagram (Fig. 4e).

Table 2
Sr, Nd and Pb isotope compositions for the İskenderun Gulf alkaline volcanic rocks.

Sample	$^{87}Sr/^{86}Sr$	2σ	$^{143}Nd/^{144}Nd$	2σ	$^{206}Pb/^{204}Pb$	2σ	$^{207}Pb/^{204}Pb$	2σ	$^{208}Pb/^{204}Pb$	2σ	$\Delta^{7/4}$	$\Delta^{8/4}$
O-2	0.703148	0.000012	0.512934	0.000005	18.7552	0.0017	15.6361	0.0015	38.6529	0.0044	11.21	35.09
O-3	0.703224	0.000012	0.512946	0.000007	19.0437	0.0014	15.6189	0.0012	38.8809	0.0035	6.35	23.00
O-16	0.703154	0.000015	0.512926	0.000003	18.9080	0.0037	15.6121	0.0030	38.7189	0.0085	7.14	23.21
O-21	0.703243	0.000018	0.512918	0.000002	19.0981	0.0031	15.6122	0.0026	38.8830	0.0062	5.10	16.63
O-24	0.703076	0.000009	0.512947	0.000003	19.0859	0.0016	15.6028	0.0013	38.8481	0.0038	4.28	14.63
O-9	0.703561	0.000017	0.512887	0.000003	19.0456	0.0049	15.6620	0.0044	39.0208	0.0106	10.64	36.77
O-12	0.703577	0.000006	0.512884	0.000001	19.0454	0.0016	15.6608	0.0011	39.0238	0.0033	10.53	37.10
O-14	0.703460	0.000009	0.512896	0.000002	19.0884	0.0054	15.6405	0.0043	38.9866	0.0103	8.03	28.17
O-30	0.703659	0.000015	0.512872	0.000002	19.0268	0.0057	15.6656	0.0039	39.0145	0.0109	11.21	38.40

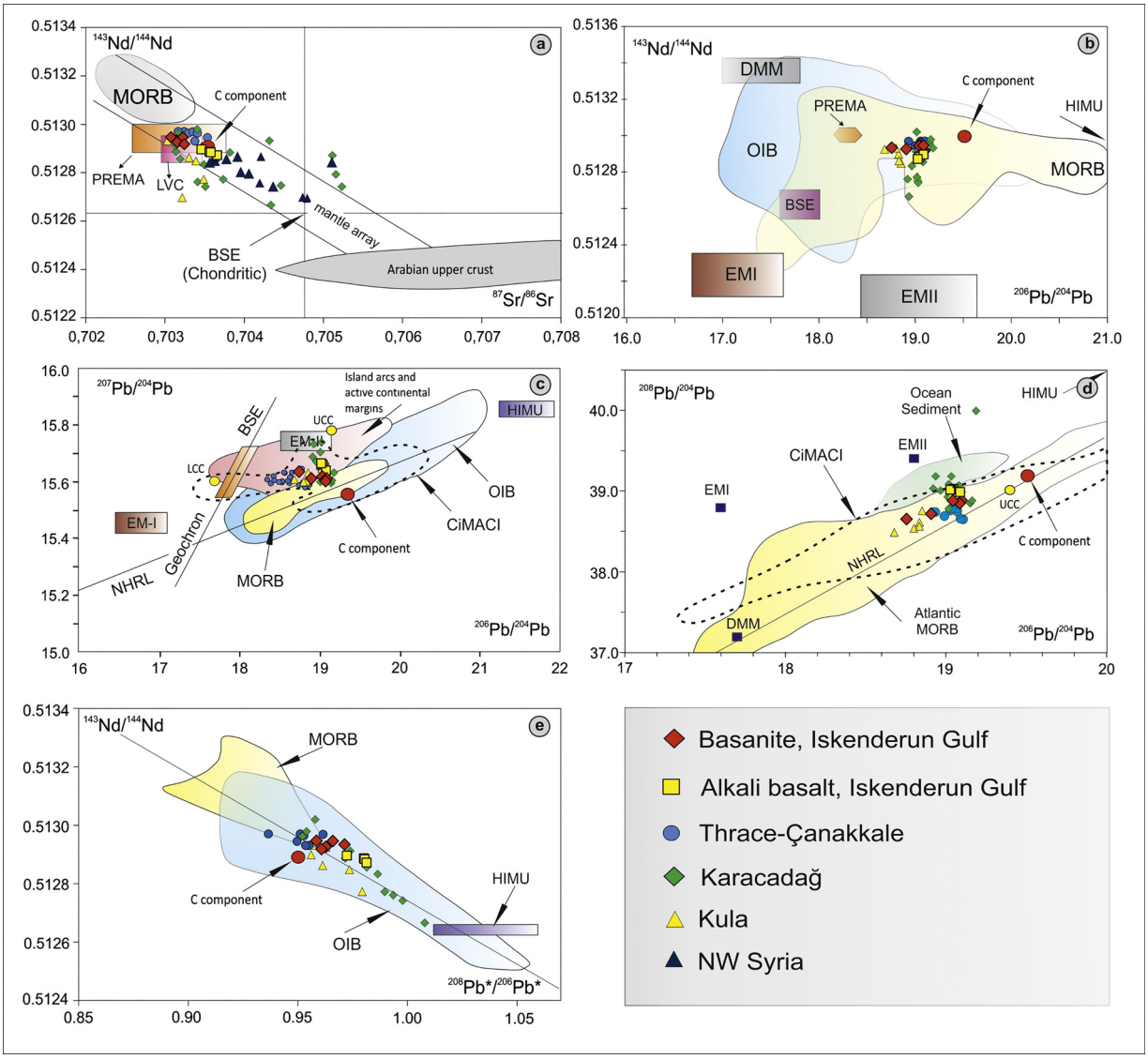

Fig. 4. (a) $^{87}Sr/^{86}Sr$ vs. $^{143}Nd/^{144}Nd$ and (b) $^{143}Nd/^{144}Nd$ vs. $^{206}Pb/^{204}Pb$ and (c) $^{207}Pb/^{204}Pb$ vs. $^{206}Pb/^{204}Pb$; and (d) $^{208}Pb/^{204}Pb$ vs. $^{206}Pb/^{204}Pb$; and (e) $^{143}Nd/^{144}Nd$ vs. $^{208}Pb^*/^{206}Pb^*$ diagrams for the alkaline lavas from Iskenderun Gulf. Data of the intra-continental volcanic rocks for a comparison is from Thrace and Çanakkale (Aldanmaz et al., 2006), Karacadağ (Keskin et al., 2012; Asan and Kurt, 2011; Şen et al., 2004), Kula (Aldanmaz et al., 2015; Alıcı et al., 2002; Innocenti et al., 2005), and NW Syria (Ma et al., 2013). Also plotted for comparison are: NHRL (Northern hemisphere reference line; Hart, 1984); common mantle component and the average composition of the upper continental crust (C, UCC; Hofmann, 1997); oceanic sediments (Ben Othman et al., 1989); Arabian upper continental crust (Hegner and Pallister, 1989; Jarrar et al., 2003); low velocity component (LVC; Hoernle et al., 1995); HIMU, EMI, and EMII (Zindler and Hart, 1986; Hart et al., 1992); the Circum-Mediterranean Anorogenic Cenozoic Igneous Province (CiMACI; Lustrino and Wilson, 2007) and Atlantic MORB (Agranier et al., 2005; Hoernle et al., 2011). The parameter $^{208}Pb^*/^{206}Pb^*$ reflects radiogenic addition to the terrestrial lead defined as [($^{208}Pb/^{204}Pb$) measured- 29.476]/[($^{206}Pb/^{204}Pb$) measured − 9.307] (Galer and O'Nions, 1985).

6. Discussion

The near primitive basaltic rocks that do not exhibit crustal contamination effect can accurately decipher the mantle composition, and in studies using such rocks the characteristics of the mantle and the processes of melting can be determined (e.g. Aldanmaz et al., 2015). In the mantle source studies using basaltic rocks, it is important to investigate the effects of shallow depth processes such as magma differentiation, contamination and mixing which are considered to change mantle trace element and isotopic signatures. For this reason, it is necessary to define whether intra-continental alkaline rocks of the İskenderun Gulf are primitive in composition and to determine the possible effects that change the composition of the primary melts.

6.1. Primary melt composition and fractional crystallization

Basaltic magmas occurring in intra-plate environments are commonly subjected to fractional crystallization at different degrees. The magmas, in this case, may differ from primitive compositions. Magmas with primitive compositions should have high concentrations of compatible trace elements (e.g. Ni, Cr, V, Sc), Mg# in the range 68–76 (e.g. Frey et al.,1978) or the bulk rock Fe/Mg ratios within a range that is in equilibrium with mantle olivine (e.g. Fo91; Albaréde, 1992). Ni and Cr (alkali basalts: 112–176 ppm; basanites: 54–322 ppm and alkali basalts: 205–342 ppm; basanites: 102–335 ppm, respectively) contents are lower than expected, and Mg# is in the range of 58–60 for alkali basalts and 52–67 for basanites. Therefore, these rocks do not appear to reflect

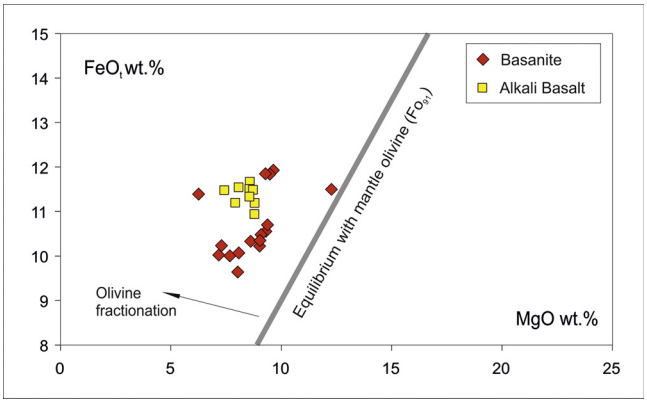

Fig. 5. Diagram of FeO_t versus MgO showing the effects of olivine fractionation on primary melt compositions. Supposing a K_D of 0.3, an Fe_2O_3/MgO ratio of 0.9 can be inferred for the melt that is in equilibrium with the mantle olivine (Fo_{91}), and the Fe_2O_3 and MgO concentrations of liquid can be estimated.

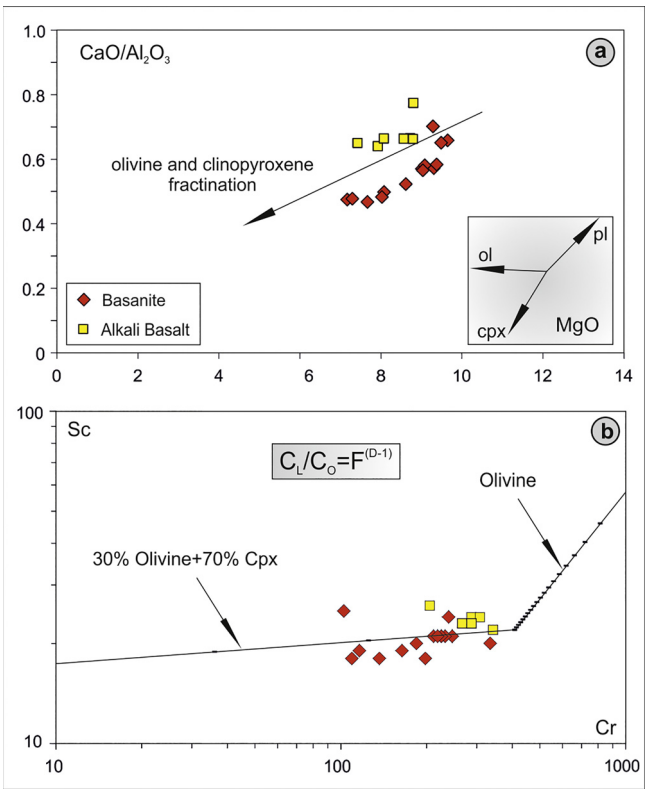

Fig. 6. (a) MgO vs CaO/Al_2O_3 diagram for volcanic rocks of the İskenderun Gulf. Diagram showing theoretical Rayleigh fractionation vectors for 50% crystallisation of the phase combinations are indicated in the inset (b) Diagram shows theoretical Rayleigh fractionation vectors for crystallization of the phase combinations. The starting composition of the vectors is taken as Sc = 22 ppm, Cr = 400 ppm. Thick marks on each vector are shown for 5% crystallization intervals. cpx = clinopyroxene.

primary melt compositions. For this reason, the rocks most likely underwent fractional crystallization at different degrees and fractionation correction is required for model studies.

To calculate the primary melt composition, the olivine control line, where the melt is in equilibrium with mantle olivine (e.g. with Fo91; Albaréde, 1992), can be considered as the reference line (Fig. 5). In Fig. 5, assuming that $K_D = [(Fe/Mg)_{ol}/(Fe/Mg)_{melt}]$ is equal to 0.3, the FeO_t/MgO = 0.9 (Albaréde, 1992) value can be determined for the melt which is in equilibrium with mantle olivine. In the diagram, primary melt composition for each sample was determined by adding olivine until the FeO_t/MgO ratio would be equal to 0.9. The amounts of olivine, F (mass fraction of liquid), fractionated from the primary melts were calculated using the determined melt compositions (where the rock compositions were used). F values were obtained by using the olivine control line and the Fe/Mg ratios of the samples. Furthermore, the changes in the MgO contents and the CaO/Al_2O_3 ratios of the samples indicate clinopyroxene and olivine fractionation; however, the fractionation of clinopyroxene is more dominant in basanites. (Fig. 6a). The genesis of the rocks can be modeled by 70% clinopyroxene + 30% olivine fractionation according to the mineral vectors attained by Rayleigh fractionation calculations using Cr, and Sc ($^{ol-lq}Kd_{Cr} \approx 0.700$, $^{cpx-lq}Kd_{Cr} \approx 34$, $^{ol-lq}Kd_{Sc} \approx 0.680$, $^{cpx-lq}Kd_{Sc} \approx 3.2$), which are hosted in olivine and clinopyroxene structures (Fig. 6b) and it is necessary to remove this effect. First, the bulk partition coefficient ($D_{70\%cpx+30\%ol}$) was calculated considering olivine and clinopyroxene fractionation. Then the primitive compositions were estimated according to Rayleigh fractionation law. The fractionation-corrected trace elements used for the melt modeling are given in Table 1.

6.2. Crustal contamination

The samples of the İskenderun Gulf intra-continental basaltic volcanism do not show negative Ta and Nb anomalies on the primitive mantle normalized diagram, indicating no significant crustal contamination (Fig. 3b). In addition, on the Th/Yb vs Ta/Yb diagram, the samples mostly plot on the diagonal mantle array indicating that the melts forming the volcanic suite have not been affected by any significant crustal contamination (Fig. 7). To test the effects of crustal involvement more precisely, the Sr-Nd isotope compositions can be used. For the modeling presented in Fig. 8 the most primitive sample was used as the initial composition, while the composition of the contaminant crust was taken as the average composition of the crustal

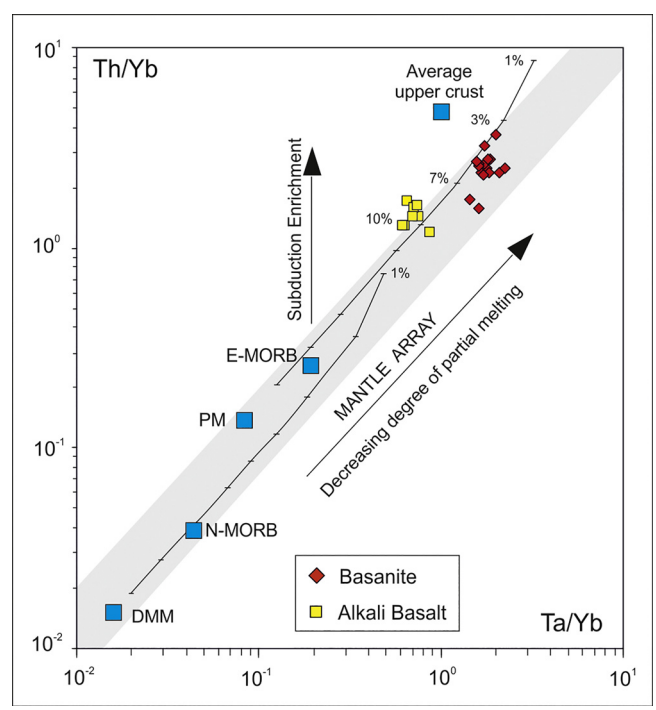

Fig. 7. Th/Yb versus Ta/Yb log-log diagram (after Pearce, 1983) for the İskenderun Gulf volcanic rocks. Some of the typical oceanic basaltic and mantle compositions including the depleted MORB mantle, primitive mantle (PM), N-MORB and E-MORB are also plotted for comparison. Average OIB and MORB values used for comparison are from Sun and McDonough (1989). The average upper crustal composition values are from Taylor and McLennan (1985).

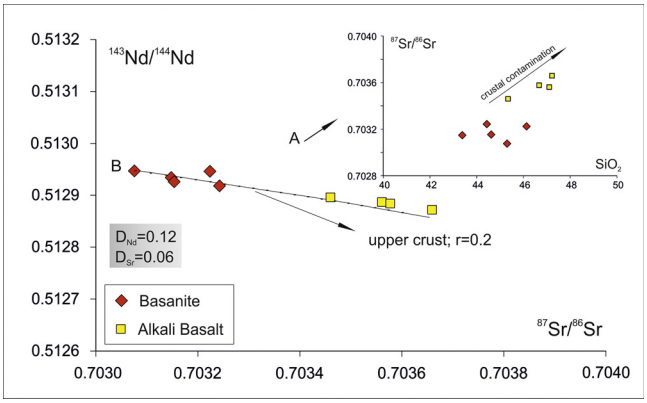

Fig. 8. Modelling of the AFC process based on the equations of DePaolo, (1981) for the İskenderun Gulf volcanic rocks, by using the Sr-Nd isotopic ratios. Crust composition is taken from the average of basement rocks (Sr = 650 ppm, Nd = 22.5 ppm, $^{87}Sr/^{86}Sr$ = 0.7064, $^{143}Nd/^{144}Nd$ = 0.5124) the Arabian Plate in Jordan (Jarrar et al., 2003). Mantle composition is taken this study (O-24; Sr = 888.6 ppm, Nd = 35.5 ppm, $^{87}Sr/^{86}Sr$ = 0.703076, $^{143}Nd/^{144}Nd$ = 0.51294). Bulk distribution coefficients are calculated using the modal mineralogy (D70% cpx + 30% ol) of volcanic rocks. The "r" value denotes the rates of mass assimilation to mass crystallization. The inset diagram shows the variation of $^{87}Sr/^{86}Sr$ vs SiO_2 for the volcanic rocks.

rocks presented in Jarrar et al. (2003). According to the AFC curve generated from these values, the alkali basalts carry a modest level of contamination (r = 0.2). Similarly, increasing ratios of $^{87}Sr/^{86}Sr$ together with increased SiO_2 content in alkali basalt support this interpretation (Fig. 8).

6.3. Characteristics of the mantle source

The intra-continental alkaline rocks of the İskenderun Gulf are highly enriched in incompatible elements. These rocks have higher $(La/Sm)_N$ of 2.8–4.2 for basanites and alkali basalts than average OIB (~2.4 Sun and McDonough, 1989), reflecting a highly enriched mantle source. Moreover, the enrichment in trace element abundances (e.g. Ta and Nb) for some of the samples compared to the primitive mantle compositions suggests melt derivation from a metasomatized mantle source. The Nd–Sr–Pb isotope compositions of these rocks indicate an origin by melting of an enriched lithospheric mantle source that was chemically modified by an OIB component (e.g. Witte et al., 2017).

Invasion of fluids from asthenosphere-derived melts or lenses of pyroxenite, amphibolite or eclogite may contribute to enrichment of LREE and LILE (Foley, 1992). Similarly, this element enrichment is associated with a metasomatized mantle such as hornblendite, carbonated peridotite and pyroxenite (e.g. Sobolev et al., 2005, 2011; Pilet et al., 2008). Geochemical and isotopic studies on OIB-like rocks point out that the possible composition of these rocks originates from a mixing of different mantle sources. For this reason, involvement of different mantle sources needs to be determined in petrogenetic studies of alkaline rocks (e.g. Sobolev et al., 2005; Niu, 2008).

The melting of metasomatized parts of the mantle can be due to either decompression through mantle upwelling or thermal perturbation in the lithosphere (Lloyd and Bailey, 1975; Wass and Rogers, 1980; Halliday et al., 1990; Pilet et al., 2008) or convective removal and delamination of the metasomatized lithosphere (e.g. in a plume; Halliday et al., 1995; McKenzie and O'Nions, 1995; Niu and O'Hara, 2003; Pilet et al., 2005). Therefore, alkaline magmas can be produced from hydrous metasomatic veins or their equivalents (Pilet et al., 2008).

Although peridotite produces alkaline melts by low degree partial melting at high pressure, a great majority of experimental mafic melts produced from peridotite do not resemble natural alkaline basalts. The experimental products have too low CaO and high Al_2O_3 compared to natural alkaline basalts (e.g. Hirschmann et al., 2003; Dasgupta et al., 2007). However, it is suggested that low MgO contents of alkaline lavas are not produced solely by fractional crystallization processes and that there should be peridotitic material bearing hydrous phases in the source. The results of melting experiments run by Foley et al. (1999) on hydrous mineral bearing veins such as amphibolite in peridotite host rock have shown that the resulting products had low MgO, SiO_2 and high Al_2O_3, TiO_2 contents. In general, experimental results obtained by Foley et al. (1999) indicate that lavas with high Ti concentrations may be produced by low-degree melting of the peridotites containing hydrous mineral phases.

In the last years, carbonated silica-poor eclogite and peridotites (Dasgupta et al., 2006, 2007) are thought to be possible sources of silica-undersaturated melts. Experimental studies supporting this idea have shown that the presence of CO_2 in mantle stabilizes orthopyroxene, and prevents it from melting and produces silica-deficient liquids. In the experiments, while the eclogite containing CO_2 produced very high FeO, CaO and CaO/Al_2O_3, the peridotite containing CO_2 produced very low FeO, SiO_2 and very high CaO, CaO/Al_2O_3 melts. In the same way, studies on both possible sources indicate that the K_2O content of melts is very low compared to the high alkali content of silica-poor mafic extrusive rocks, and that the compositions of melts produced by carbonated sources show variations according to the composition of OIB-type rocks (Dasgupta et al., 2007). The high Ti contents of most alkaline OIB can be explained by a metasomatized source that can increase the Ti and alkali concentration of the source (Prytulak and Elliott, 2007). For example, the geochemical composition of high Ti amphibole xenocrysts in the Rhön basalts of the CEVP (Central European Volcanic Province) resembles those of the amphibole veins in the lithospheric mantle and from this it follows that high-Ti alkaline rocks are likely generated from metasomatized mantle sources (Mayer et al., 2014).

Silica-poor pyroxenite is recognized as a source for mafic alkaline magmas, while SiO_2-enriched pyroxenite is considered as a possible source for tholeiitic magmas (e.g. Hirschmann et al., 2003; Keshav et al., 2004; Zhang et al., 2009). The source lithologies of alkaline magmas are highly enriched in incompatible element such as K, Ba, Rb, and LREE relative to the peridotitic mantle. Silica-poor garnet pyroxenites do not have such enriched trace element concentrations and recycled oceanic crust cannot provide enrichment in this way (Stracke et al., 2003). Only metasomatic processes are expected for such enrichment (e.g. Nielson and Noller, 1987; Harte et al., 1993; Nielson and Wilshire, 1993).

The TiO_2-rich mantle xenoliths within the alkaline volcanic rocks may occur in pyroxenite veins which are influenced by the involvement of basaltic melts (Witt-Eickschen et al., 1993). On the other hand, Pilet et al. (2008) proposed that the K_2O concentration of alkaline rocks cannot be clarified by silica-poor pyroxenite as a mantle source. Sobolev et al. (2007) indicated that pyroxenite-originated melts are rich in Si and Ni but depleted in Mg, Ca and Mn compared to peridotites. For this reason, such a source cannot explain the concentrations of trace elements and K_2O content in the alkaline basalts of the İskenderun Gulf.

Potassium and TiO_2 enrichment of the alkaline rocks can be explained by phases such as K and Ti-rich amphibole or phlogopite (Foley et al., 1996; Pilet et al., 2008) in the mantle source. The relative abundances of alkaline elements in the volcanic rocks can be used to determine the existence of amphibole or phlogopite in the mantle source as these elements have different partitioning behavior during partial melting. As a result of the incompatibility differences, the melts in equilibrium with phlogopite have considerably higher Rb/Sr (> 0.1) and lower Ba/Rb (< 20) than the amphibole-bearing mantle sources (Rb/Sr < 0.06; Ba/Rb > 20; Furman and Graham, 1999).

While Rb depletion in all samples is apparent, a significant enrichment in Ba (Fig. 3b) shows the effect of these potassic/hydrous phases in the source. The rocks have high Ce/Pb ratios (~26-80) from the presumed range for OIB (Ce/Pb = 25+/-5; Hofmann et al., 1986) due

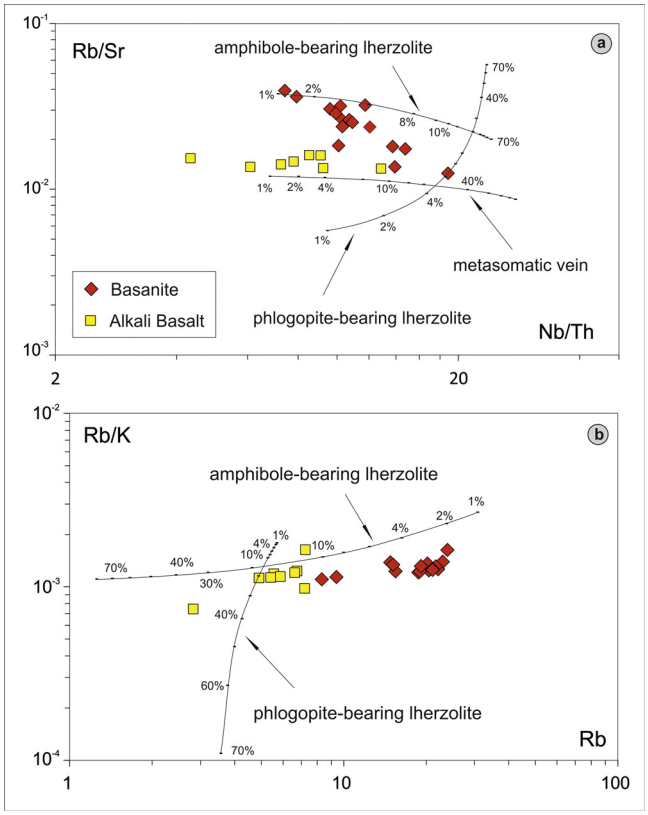

Fig. 9. (a) Nb/Th vs. Rb/Sr, (b) Rb vs. Rb/K covariation for the İskenderun Gulf alkaline rocks. Partial melting curves were calculated using the non-modal batch partial melting of Shaw (1970). Melt trajectories are drawn for amphibole-bearing lherzolite (with mode and melt mode of $ol_{0.550} + opx_{0.19} + cpx_{0.07} + gt_{0.08} + amp_{0.11}$ and $ol_{0.05} + opx_{0.15} + cpx_{0.10} + gt_{0.3} + amp_{0.25}$; respectively; Witt-Eickschen et al., 1993); and phlogopite-bearing lherzolite (with mode and melt mode of $ol_{0.564} + opx_{0.188} + cpx_{0.141} + gt_{0.047} + phl_{0.06}$ and $ol_{0.17} + opx_{0.19} + cpx_{0.27} + gt_{0.02} + phl_{0.35}$; respectively; Duggen et al., 2005) and amphibole metasomatic vein (with mode and melt mode of $gt_{0.05} + amp_{0.95}$ and $cpx_{-0.14} + gt_{-0.16} + amp_1$; respectively; Pilet et al., 2008). The source compositions calculated using the dynamic melting inversion method proposed by Zou and Zindler (1996); Nb = 2.57 ppm; Th = 0.11 ppm; Rb = 0.85 ppm, Sr = 39.47 ppm; K = 692 ppm. Partition coefficients used are from the compilation of McKenzie and O'Nions (1991, 1995), Green (1994) and LaTourrette et al. (1995).

to low Pb concentrations (0.8–2.9 ppm). It is generally supposed that amphibole and phlogopite are the main phases for Pb in the mantle (Rosenbaum, 1993). Thus, mantle melting that leaves amphibole or phlogopite-bearing residues would likely produce melts depleted in Pb. The low Rb/Sr (0.01-0.04) and high Ba/Rb (9.7–40.7) ratios of the mafic alkaline samples show that the main phase was amphibole in mantle source. In addition, Pilet et al. (2010) indicated that the melting temperature remarkably changes the Al_2O_3 and MgO abundance of the melt. Melting at low temperatures causes lower MgO but higher Al_2O_3 abundances in the melt, compared to common alkali basalts with similar SiO_2 and minor variations of TiO_2 contents (e.g. Mayer et al., 2013).

The Nb/Th vs. Rb/Sr variation suggested by Furman and Graham (1999) can also be used to test whether the hydrous phases in the mantle source is amphibole or phlogopite (Fig. 9a). Here, the Nb/Th ratios of the samples may be controlled by the hydrous phase as Nb is more compatible in amphibole than phlogopite ($^{amp}Kd_{Nb} = 0.159$, $^{phl}Kd_{Nb} = 0.085$; LaTourrette et al., 1995). The Nb/Th ratio in most of the samples increases with decreasing Rb/Sr ratio. In Fig. 9a, the samples also plot between the melting curves defined for amphibole-bearing lherzolite and amphibolite vein and this may indicate the existence of residual amphibole in the mantle source during the melting process. Similarly, Rb/K vs. Rb variations may provide an additional constraint in defining the possible hydrous phase in the mantle residue. Since K is less compatible in amphibole than in phlogopite ($^{amp}Kd_K = 0.58$, $^{phl}Kd_K = 3.67$; LaTourrette et al., 1995), melting of the amphibole-bearing lherzolite would not much affect the Rb/K ratio, while this ratio is affected significantly during melting in the presence of residual phlogopite. The increase in Rb abundances and insignificant change in Rb/K ratios of the samples on the diagram, therefore, further support amphibole-bearing lherzolite source rather than phlogopite-bearing source (Fig. 9b).

Combined together, it can be considered that hornblendite or amphibole-rich veins may be a more suitable source for alkaline rocks of the İskenderun Gulf. Pilet et al. (2008) used experiments in amphibole-bearing metasomatic veins at 1.5 GPa to suggest that partial melting of amphibole-rich parts of the mantle would reflect the geochemical properties of continental and oceanic alkaline magmas. These melting experiments have shown that amphibole-bearing veins represent the source which may produce large fraction of melt due to its low solidus temperature. These melts have high alkalis and TiO_2 and show high LREE/HREE (e.g. $(La/Yb)_N > 5$) at reasonable level and intermediate MREE/HREE (e.g. $(Dy/Yb)_N > 1.6$) along with Rb, K, Pb, and Zr anomalies in the primitive mantle normalized diagrams.

Partial melting of amphibole-rich veins, such as hornblendite, cpx-hornblendite and hornblendite + peridotite sandwiches, may generally produce mafic melts with high alkali content. Especially, the partial melting of the hornblendite + peridotite sandwich can produce mafic melts with high SiO_2 content (Dai et al., 2014). On the other hand, the pure hornblendite melts have very low content of SiO_2 in comparison to alkaline rocks of the İskenderun Gulf.

Using the trace element partition coefficients, the partial melting conditions of the source of parental İskenderun Gulf alkaline rocks can be modeled and the compositional variations of these alkaline magmas resulting in a mixture between amphibole-bearing peridotite and peridotite melts can be tested (e.g Ma et al., 2011a). In the Dy/Yb vs La/Yb diagram, non-modal batch melting models were used to constrain the melting regime and the involvement of garnet in the source (Fig. 10). The peridotite and amphibole-bearing peridotite compositions and their modal compositions are given in Table 3. Primitive mantle compositions (Sun and McDonough, 1989) were used for peridotite and

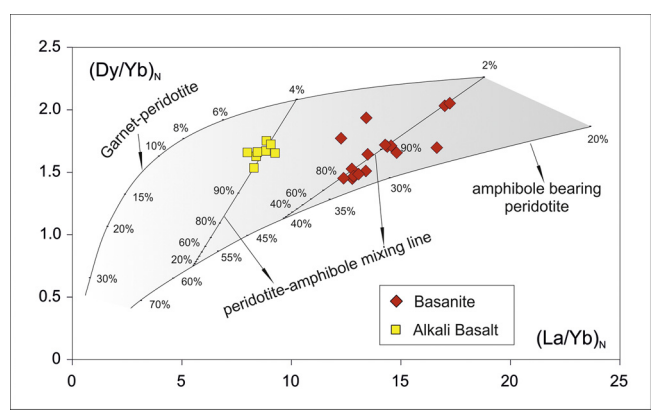

Fig. 10. La/Yb vs. Dy/Yb covariation for the İskenderun Gulf alkaline rocks. The continuous curves show non-modal batch melting models for peridotite (with a primitive mantle composition) and amphibole-bearing peridotite metasomatic vein as starting materials. It should be noted that most basalt samples fall in the grey-shaded fields, which define the possible melt compositions from mixing of small-degree (F = 2–4%) peridotite melts and large-degree (F = 40–60%) amphibole-bearing peridotite metasomatic vein melts. Source compositions and partition coefficient values are given in Table 3. F = degree of partial melting.

Table 3
Mineral-melt partition coefficients, source compositions and source modes used in partial melting modelling.

Partition coefficient							
	Ol	Opx	Cpx	Gt	Amp	Source (ppm)	
						PM	vein
La	0.0004	0.002	0.054	0.01	0.17	0.687	52.7
Yb	0.0015	0.049	0.28	4.03	0.59	0.493	2.54
Dy	0.022	0.33	0.055	1	0.78	0.737	7

Source Mode	Ol	Opx	Cpx	Gt	Amp
Garnet-bearing lherzolite					
Mineral mode	0.598	0.211	0.076	0.115	
Melting mode	0.05	0.20	0.30	0.45	
Garnet-bearing amphibole metasomatic vein					
Mineral mode	0.550	0.19	0.07	0.08	0.11
Melting mode	0.05	0.15	0.10	0.30	0.25

Ol, olivine; Opx, orthopyroxene; Cpx, clinopyroxene; Gt, garnet; Amph, amphibole; PM, primitive mantle of Sun and McDonough (1989); metasomatic vein, AG4 (Pilet et al., 2008). Garnet bearing lherzolite are taken from Thirlwall et al. (1994). Garnet-bearing amphibole is taken from (Witt-Eickschen et al., 1998); mineral/matrix partition coefficients are from the compilation of McKenzie and O'Nions (1991, 1995).

amphibole-bearing peridotite source components in the calculations. The use of the primitive mantle composition does not mean that the source is the primordial mantle. Compared to bulk earth, the samples having slightly decreased Sr, increased Nd isotopic ratios indicating long-term depletion in the source. Therefore, this primitive mantle composition should mirror a re-fertilized mantle source initially depleted but subsequently enriched by melts that are probably close to a primitive mantle composition or are enriched in incompatible elements (Ma et al., 2011a).

The Dy/Yb ratio of melt is normally controlled by garnet, because of the high compatibility of HREE in garnet. The Dy/Yb ratio can be decreased by the addition of amphibole due to the higher MREE compatibility in amphibole. Most of the samples plot between the peridotite and amphibole-bearing peridotite melting curves calculated by the melting model. They can be interpreted as the products of varying degrees of mixing between amphibole-bearing peridotite-derived (~40–60% melt fractions) and peridotite-derived melts (~2–4% melt fractions). According to this melting model, contribution of the amphibole-bearing metasomatic veins in the alkaline basalts of the İskenderun Gulf is approximately 40% or more.

6.4. Development of the metasomatised source region

Metasomatic veins rich in amphibole, which appear to be the main source of common alkaline magmas (Pilet et al., 2008, Pilet et al., 2011; Ma et al., 2011a, b) are usually considered to have formed in the lithospheric mantle during melt ascent and migration. The interaction of hydrous melt-peridotite (Rapp et al., 1999; Prouteau et al., 2001) produces these veins which also contain xenoliths derived from different depths in mantle (e.g. Downes et al., 2004; Powell et al., 2004). Melts derived from such veins are strongly silica-undersaturated, but when these melts react with the orthopyroxene in the host peridotite, partially siliceous olivine-rich mafic melts form (Hirschmann et al., 2003; Pilet et al., 2008).

Anhydrous and hydrous metasomatic veins are interpreted as being produced during progressive differentiation of primary hydrous alkaline magmas at high pressure. The comparison between the products formed by fractional crystallization of Ne-normative or Hy-normative initial compositions (hawaiite or picrobasalt) shows that all hydrous liquids generated by differentiation are generally similar. For this reason, it has been suggested that the development of amphibole-bearing metasomatic veins in lithospheric mantle may be related to the change of the initial melts from Ne-normative to Hy-normative (Pilet et al., 2010). However, percolation and differentiation of a liquid produced at a low degree of partial melting of a mantle source enriched slightly or similar to MORB supports the possibility of hydro-metasomatic veins being interpreted elsewhere as a possible source for alkaline magmatism.

Niu (2008, 2009), and Humphreys and Niu (2009) suggested that H_2O and CO_2-rich primary melts migrating upward would metasomatize the base of the lithosphere with a melt-rich level above the low velocity zone (LVZ). High-pressure equilibrium crystallization experiments in hydrous, CO_2-containing basanitic melts show that mainly cpx-dominated, anhydrous mineral assemblages such as olivine ± garnet ± orthopyroxene in varying amounts occur in the host rock because of percolation processes in the lithosphere (e.g. Harte et al., 1993; Pilet et al., 2010). However, amphibole crystallized predominantly in the residual melts due to varying composition of the melts with more percolation of melts. Finally, hydrous crystallizing assemblages in addition to amphibole may contain various secondary phases such as clinopyroxene ± plagioclase ± phlogopite ± orthopyroxene ± garnet, and rutile and apatite. The compositions of amphiboles derived from metasomatic veins are similar to those of amphiboles that crystallized in FC experiments. In this case, the metasomatic veins are interpreted to have developed during the differentiation of the primary or derivative melts in the lithospheric mantle (Pilet et al., 2010). In addition, the solidus temperatures of amphibole-bearing metasomatic veins (e.g. Pilet et al., 2008) are considered to be lower than those of the anhydrous assemblages (garnet + clinopyroxene ± olivine) forming the surrounding peridotite matrix.

6.5. Geodynamic Implications and cause of mantle melting

Boundaries between Africa, Arabia and Eurasian plates are irregular in the Mediterranean region and geodynamics of the region is determined by the relative movements of the plates. Bitlis suture constitutes the border between Anatolia and Arabia plates and a thrust in the northern part of the Amanos constitutes the border between Anatolia and Africa (Chorowıcz et al., 1994). The Dead Sea Fault Zone, developed due to the movements of Africa, Arabia and Eurasia plates, starts from the Red Sea and Maraş extends to the triple junction and the Bitlis suture zone (Fig. 1). Trans-tensional movements along the Dead Sea fault zone cause lithospheric extension (Lustrino and Sharkov, 2006). The alkali volcanism of the İskenderun Gulf exists on the plate

boundaries of Africa-Arabia and lies along the active left-lateral northeast-southwest trending Karatas-Osmaniye Fault Zone (Yurtmen et al., 2000).

In the south of Turkey, the trace element concentrations of the mafic extrusive rocks of the İskenderun Gulf are explained by the metasomatic nature of the source. Although the samples have high Rb/Sr and low Sm/Nd ratios, the Sr-Nd isotopic signature ($^{87}Sr/^{86}Sr$ = 0.7031-0.7036 and $^{143}Nd/^{144}Nd$ = 0.5218-0.5129) points rather towards a depleted source, suggesting a young age for the metasomatism. The geochemical characteristics of the rocks imply hydrous metasomatized veins and the mixing of these veins with peridotites, and low solidus temperatures are sufficient for the melting of such a source. These types of metasomatized mantle components containing amphibole-bearing vein assemblages have also been proposed to be the main source of the alkaline basaltic suites located further south in north-western Syria and in Israel, where hornblendite mantle xenoliths have been reported (e.g. Downes et al., 2004).In addition, experimental studies on the pressures over 3 GPa suggested that there is a significant change in the upper mantle water storage capacity (dropping from ~ 0.3-0.4 wt% to 180 ppm) due to pargasite instability (Green et al., 2010, 2011). The depth that corresponds to this pressure (~100 km) indicates the lithosphere-asthenosphere boundaries of a mature oceanic lithosphere as well as the non-cratonic continental lithosphere in the region. Ma et al. (2013) suggested that hydrous interstitial melts present at the boundary of the lithosphere-asthenosphere are responsible for the seismic low-velocity zone observed under many mature ocean basins and in much of Northwest and Western Arabia (Ma et al., 2013). Upward migration of hydrous melts during localized lithospheric extension in the region provides a reasonable mechanism for the evolution of metasomatic veins which produced the alkaline volcanism of the İskenderun Gulf due to decompressional melting caused by trans-tensional tectonism in the region.

7. Conclusions

The alkaline rocks of the İskenderun Gulf with low silica content are classified as basanite and alkali basalt, being sodic and nepheline-normative in composition. Fractionation vectors calculated theoretically from trace element data indicate that clinopyroxene and olivine are the main mineral phases in crystallization assemblages of the rocks. The Sr, Nd and Pb isotopic characteristics of volcanic rocks are similar to those of other occurrences with OIB affinity in the region and NW Syria. The Sr-Nd isotopic data and the assimilation and fractional crystallization (AFC) models suggest that alkali basalts were slightly contaminated by the upper crust material. High TiO_2 and Al_2O_3 contents combined with radiogenic isotope and trace element characteristics show the effect of metasomatized veins in the formation of OIB-type magmas. Trace element modeling shows variable degrees of mixing between amphibole-bearing peridotite and peridotite-derived melts and the involvement of metasomatic veins containing at least 40% amphibole-bearing peridotite in the source of the İskenderun Gulf alkaline rocks. The alkali basalts and basanitic rocks are generated by different extent of mixing of these sources. The decompressional melting due to trans-tensional tectonic in metasomatic veins is the major process for formation of the alkaline rocks of the İskenderun Gulf.

Acknowledgements

This research was financially supported by the Research Fund of Kocaeli University (Project No: 2014/84, 2015/19). The author thanks Dr. Ercan Aldanmaz for his valuable contributions to this work. I thank S. Jung and V. Rapprich for constructive journal reviews. I am also grateful to Tomas Magna for his efficiency and helpfulness as referee and editor.

References

Ackerman, L., Špaček, P., Magna, T., Ulrych, J., Svojtka, M., Hegner, E., 2013. Alkaline and carbonate-rich melt metasomatism and melting of subcontinental lithospheric mantle: evidence from mantle xenoliths, NE Bavaria, Bohemian Massif. J. Petrol. 54, 2597–2633.
Adıyaman, Ö., Chorowicz, J., 2002. Late Cenozoic tectonics and volcanism in the northwestern corner of the Arabian Plate: A consequence of the strike slip Dead Sea Fault Zone and the lateral escape of Anatolia. J. Volcanol. Geotherm. Res. 249, 1–19.
Agranier, A., Blichert-Toft, J., Graham, D., Debaille, V., Schiano, P., Albarède, F., 2005. The spectra of isotopic heterogeneities along the Mid-Atlantic Ridge. Earth Planet. Sci. Lett. 238, 96–109.
Albaréde, F., 1992. How deep do common basalts form and differentiate? J. Geophys. Res. 97, 10997–11009.
Albora, M., Sayın, N., Uçan, O.N., 2006. Evaluation of tectonic structure of Iskenderun Basin (Turkey) using steerable filters. Mar. Geophys Res. 27, 225–239.
Aldanmaz, E., 2002. Mantle source characteristics of alkali basalts and basanites in an extensional intracontinental plate setting, western Anatolia, Turkey: implication for multi-stage melting. Int. Geol. Rev. 44, 440–457.
Aldanmaz, E., Köprübaşı, N., Gürer, Ö.F., Kaymakçı, N., Gourgaud, A., 2006. Geochemical constraints on the Cenozoic, OIB-type alkaline volcanic rocks of NW Turkey: implications for mantle sources and melting processes. Lithos 86, 50–76.
Aldanmaz, E., Pickard, M., Meisel, T., Altunkaynak, Ş., Sayıt, K., Şen, P., Hanan, B.B., Furman, T., 2015. Source components and magmatic processes in the genesis of Miocene to Quaternary lavas in western Turkey: constraints from HSE distribution and Hf–Pb–Os isotopes. Contrib. Mineral. Petrol. 170, 1–20.
Alıcı, P., Temel, A., Gourgaud, A., 2002. Pb–Nd–Sr isotope and trace element geochemistry of Quaternary extension related alkaline volcanism: a case study of Kula region (western Anatolia, Turkey). J. Volcanol. Geotherm. Res. 115, 487–510.
Arger, J., Mitchell, J., Westaway, R.W.C., 2000. Neogene and Quaternary Volcanism of Southeastern Turkey 173. Geological Society, London, Special Publications, pp. 459–487.
Asan, K., Kurt, H., 2011. Petrology and geochemistry of post-collisional Early Miocene volcanism in the Karacadağ area (CentralAnatolia, Turkey). Acta Geologica Sinica-English Edition 85, 1100–1117.
Bağcı, U., Alpaslan, M., Frei, R., Kurt, M.A., Temel, A., 2011. Different degrees of partial melting of the enriched mantle source for plio−Quaternary basic volcanism, Toprakkale (Osmaniye) region, Southern Turkey. Turkish J. Earth Sci 20, 115–135.
Bayer, H.J., Hotzl, H., Jado, A.R., Rocher, B., Voggenreiler, W., 1988. Sedimentery and structural evolution of the northwest Arabian Red Sea Margin. Tectonophysics 204, 1–15.
Ben Othman, D., White, W.M., Patchett, J., 1989. The geochemistry of marine sediments, island arc magma genesis and crust-mantle recycling. Earth Planet. Sci. Lett. 94, 1–21.
Boynton, W.V., 1984. Geochemistry of the rare earth elements: meteorite studies. In: Henderson, P. (Ed.), Rare Earth Element Geochemistry. Elsevier, pp. 63–114.
Cas, R.A.F., Wright, J.V., 1987. Volcanic Successions: Modern and Ancient. Allen and Unwin, London, pp. 528.
Chorowıcz, J., Luxey, P., Lyberis, N., Carvalho, J., Parrot, J.F., Yürür, T., Gündogdu, M.N., 1994. The Maraş Triple Junction southern Turkey. Based on digital elevation model and satel-lite imagery interpretation. J. Geophys Reaserch 99, 20225–20242.
Dai, L.Q., Zhao, Z.F., Zheng, Y.F., 2014. Geochemical insights into the role of metasomatic hornblendite in generating alkali basalts. Geochem. Geophys. Geosyst. 15, 3762–3779.
Dasgupta, R., Hirschmann, M.M., Stalker, K., 2006. Immiscible transition from carbonate-rich to silicate-rich melts in the 3GPa melting interval of eclogite + CO_2 and genesis of silica undersaturated ocean island lavas. J. Petrol. 47, 647–671.
Dasgupta, R., Hirschmann, M.M., Smith, N.D., 2007. Partial melting experiments of peridotite 1CO_2 at 3 GPa and genesis of alkalic ocean island basalts. J. Petrol. 48, 2093–2124.
DePaolo, D.J., 1981. Trace element and isotopic effects of combined wall rock assimilation and fractional crystallization. Earth Planet. Sci. Lett. 53, 189–202.
Downes, H., Beard, A., Hinton, R., 2004. Natural experimental charges: an ion-microprobe study of trace element distribution coefficients in glass-rich hornblendite and clinopyroxenite xenoliths. Lithos 75, 1–17.
Duggen, S., Hoernle, K., Bogaard, P.V.D., GarbeSchönberg, D., 2005. Post-collisional transition from subduction- to intraplate-type magmatism in the westernmost Mediterranean: evidence for continental-edge delamination of subcontinental lithosphere. J. Petrol. 46, 1155–1201.
Foley, S., 1992. Vein-Plus-Wall-Rock melting mechanisms in the lithosphere and the origin of potassic alkaline magmas. Lithos 28 (3-6), 435–453.
Foley, S.F., Jackson, S.E., Fryer, J.D., Greenough, G.A.J., 1996. Trace element partition coefficients for clinopyroxene and phlogophite in an alkaline lamprophyre from Newfoundland by LAM-ICP-MS. Geochim. Cosmochim. Acta 60, 629–638.
Foley, S., Musselwhite, D.S., van der Laan, S.R., 1999. Melt compositions from ultramafic vein assemblages in the lithospheric mantle: a comparison of cratonic and non-cratonic settings. In: Gurney, J.J., Gurney, J.L., Pascoe, M.D., Richardson, S.H. (Eds.), Proceedings of the 7th International Kimberlite Conference. Red Roof Design. pp. 238–246.
Frey, F.A., Green, D.H., Roy, S.D., 1978. Integrated models of basalt petrogenesis: a study of quartz tholeiites to olivine melilitites from SE Australia utilizing geochemical and experimental petrological data. J. Petrol. 19, 463–513.
Furman, T., Graham, D., 1999. Erosion of lithospheric mantle beneath the East African Rift system: geochemical evidence from the Kivu volcanic province. Lithos 48, 237–262.

Fyitkas, M., Innocenti, F., Manetti, P., Peccerillo, A., Villari, L., 1984. Tertiary to quaternary evolution of volcanism in the aegean region. In: In: Dixon, J.E., Robertson, A.H.F. (Eds.), The Geological Evolution of the Eastern Mediterranean. 17. Geological Society of London, Special Publication, pp. 687–699.
Galer, S.J.G., O'Nions, R.K., 1985. Residence time of thorium, uranium and lead in the mantle with implications for mantle convection. Nature 316, 778–782.
Green, T.H., 1994. Experimental studies of trace-element partitioning applicable to igneous petrogenesis-Sedona 16 years later. Chem. Geol. 117, 1–36.
Green, D.H., Hibberson, W.O., Kovács, I., Rosenthal, A., 2010. Water and its influence on the lithosphere–asthenosphere boundary. Nature 467, 448–451.
Green, D.H., Hibberson, W.O., Kovács, I., Rosenthal, A., 2011. Addendum: water and its influence on the lithosphere–asthenosphere boundary. Nature 472, 504.
Gürsoy, H., Tatar, O., Piper, J.D.A., Heimann, A., Mesci, L., 2003. Neotectonic deformation in the Gulf of Iskenderun, Southern Turkey, deduced from paleomagnetıc study of the Ceyhan–Osmaniye Volcanics. Tectonics 22 (6), 1–11.
Gürsoy, H., Tatar, O., Piper, J.D.A., Heimann, A., Koçbulut, F., Mesci, B.L., 2009. Palaeomagnetic study of Tertiary volcanic domains in Southern Turkey and Neogene anticlockwise rotation of the Arabian Plate. Tectonophysics 465 (1), 114–127.
Halliday, A.N., Davidson, J.P., Holden, P., DeWolf, C., Lee, D.C., Fitton, J.G., 1990. Trace-element fractionation in plumes and the origin of HIMU mantle beneath the Cameroon line. Nature 347, 523–528.
Halliday, A.N., Lee, D.-C., Tommasini, S., Davies, G.R., Paslick, C.R., Fitton, J.G., James, D.E., 1995. Incompatible trace elements in OIB and MORB and source enrichment in the sub-oceanic mantle. Earth Planet. Sci. Lett. 133, 379–395.
Hart, S.R., 1984. A large-scale isotope anomaly in the southern hemisphere mantle. Nature 309, 753–757.
Hart, S.R., 1988. Heterogeneous mantle domains: signatures, genesis and mixing chronologies. Earth Planet. Sci. Lett. 90, 273–296.
Hart, S.R., Hauri, E.H., Oschmann, L.A., Whitehead, J.A., 1992. Mantle plumes and entrainment: isotopic evidence. Science 256, 517–520.
Harte, B., Hunter, R.H., Kinny, P.D., 1993. Melt geometry, movement and crystallization, in relation to mantle dykes, veins and metasomatism. Philosophical Transaction of the Royal Society of London Series A342. pp. 1–21.
Hawkesworth, C.J., Gallagher, K., 1993. Mantle hotspots, plumes and regional tectonics as causes of intraplate magmatism. Terra Nova 5 (6), 552–559.
Hegner, E., Pallister, J.S., 1989. Pb, Sr, and Nd isotopic characteristics of Tertiary Red Sea Rift volcanics from the central Saudi Arabian coastal plain. J. Geophys. Res. 94, 7749–7755.
Hirschmann, M.M., Kogiso, T., Baker, M.B., Stolper, E.M., 2003. Alkalic magmas generated by partial melting of garnet pyroxenite. Geology 31, 481–484.
Hoernle, K., Zhang, Y.-S., Graham, D., 1995. Seismic and geochemical evidence for large-scale mantle upwelling beneath the eastern Atlantic and western and central Europe. Nature 374, 34–39.
Hoernle, K., Hauff, F., Kokfelt, T.F., Haase, K., Garbe-Schönberg, D., Werner, R., 2011. On- and off-axis chemical heterogeneities along the South Atlantic Mid-Ocean-Ridge (5–11°S): shallow or deep recycling of ocean crust and/or intraplate volcanism? Earth Planet. Sci. Lett. 306, 86–97.
Hofmann, A.W., 1997. Mantle geochemistry: the message from oceanic volcanism. Nature 385 (16), 219–229.
Hofmann, A.W., White, W.M., 1982. Mantle plumes from ancient oceanic crust. Earth Planet. Sci. Lett. 57, 421–436.
Hofmann, A.W., Jochum, K.P., Seufert, M., White, W.M., 1986. Nb and Pb in oceanic basalts: new constraints on mantle evolution. Earth Planet. Sci. Lett. 79, 33–45.
Humphreys, E.R., Niu, Y., 2009. On the composition of ocean island basalts (OIB): the effects of lithospheric thickness variation and mantle metasomatism. Lithos 112, 118–136.
Innocenti, F., Agostini, S., Di Vincenzo, G., Doglioni, C., Manetti, P., Savaşçın, M.Y., Tonarini, S., 2005. Neogene and Quaternary volcanism in western Anatolia: magma sources and geodynamic evolution. Mar. Geol. 221, 397–421.
İzzeldin, A.Y., 1987. Seismic gravity and magnetic surveys in central part of the Red Sea: their interpretation and implications for the structure and evolution of the Red Sea. Tectonophysics 143, 269–306.
Jarrar, G., Stern, R.J., Saffarine, G., Al-Zubi, H., 2003. Late- and post-orogenic Neoproterozoic intrusions of Jordan: implications for crustal growth in the northernmost segment of the East African Orogen. Precambrian Res. 123, 295–319.
Karig, D.E., Kozlu, H., 1990. Late Palaeogene- Neogene evolution of the triple junction region near Maras, south-central Turkey. J. Geological Soc. London 147, 1023–1034.
Kelling, G., Gökçen, S.L., Floyd, P.A., Gökçen, N., 1987. Neogene tectonics and plate convergence in the eastern Mediterranean: new data from southern Turkey. Geology 15, 425–429.
Kempton, P., Harmon, R., Stosch, H.G., Hoefs, J., Hawkesworth, C., 1988. Open-system O-isotope behaviour and trace element enrichment in the sub-Eifel mantle. Earth Planet. Sci. Lett. 89, 273–287.
Keshav, S., Gudfinnsson, G.H., Sen, G., Fei, Y., 2004. High-pressure melting experiments on garnet clinopyroxenite and the alkalic to tholeiitic transition in ocean-island basalts. Earth Planet. Sci. Lett. 223, 365–379.
Keskin, M., Chugaev, A., Lebedev, V.A., Sharkov, E., Oyan, V., Kavak, O., 2012. The geochronology and origin of mantle sources for late cenozoic intraplate volcanism in the frontal part of the arabian plate in the Karacada Neovolcanic Area of Turkey. Part 2. The results of geochemical and isotope (Sr–Nd–Pb) studies. J. Volcanol. Seismol. 6, 361–382.
Kozlu, H., 1987. Misis–Andırın Dolaylarının Stratigrafisi ve yapısal evrimi. Türkiye Petrol Kongresi Dergisi 7, 104–116.
LaTourrette, T., Hervig, R.L., Holloway, J.R., 1995. Trace element partitioning between amphibole, phlogopite, and basanite melt. Earth Planet. Sci. Lett. 135, 13–30.
Le Bas, M.J., Le Maitre, R.W., Streckeisen, A., Zanettin, B., 1986. A chemical classification of volcanic rocks based on the total alkali–silica diagram. J. Petrol. 27, 445–450.
Le Pichon, X., Gaulier, J.M., 1988. The rotation of Arabia and the Levant Fault system. Tectonophysics 153, 271–294.
Lloyd, F.E., Bailey, D.K., 1975. Light element metasomatism of the continental mantle: the evidence and the consequences. In: Ahrens, L.H., Dawson, J.B., Duncan, A.R., Erlank, A.J. (Eds.), Physics and Chemistry of the Earth 9. Pergamon Press, Oxford, pp. 389–416.
Lustrino, M., Sharkov, E., 2006. Neogene volcanic activity of western Syria and its relationship with Arabian plate kinematics. J. Geodyn. 42, 115–139.
Lustrino, M., Wilson, M., 2007. The circum-Mediterranean anorogenic Cenozoic igneous province. Earth. Rev. 81, 1–65.
Ma, G.S.-K., Malpas, J., Xenophontos, C., Chan, G.H.N., 2011a. Petrogenesis of latest Miocene–quaternary continental intraplate volcanism along the northern Dead Sea Fault System (Al Ghab–homs Volcanic Field), western Syria: evidence for lithosphere–asthenosphere interaction. J. Petrol. 52, 401–430.
Ma, G.S.-K., Malpas, J., Xenophontos, C., Suzuki, K., Lo, C.-H., 2011b. Early cretaceous volcanism of the coastal ranges, NW Syria: magma genesis and regional dynamics. Lithos 126, 290–306.
Ma, G.S.-K., Malpas, J., Suzuki, K., Lo, C.-H., Wang, K.L., Iizuka, Y., Xenophontos, C., 2013. Evolution and origin of the miocene intraplate basalts on the Aleppo Plateau, NW Syria. Chem. Geol. 335, 149–171.
Mayer, B., Jung, S., Romer, R.L., Stracke, A., Haase, K.M., Garbe-Schönberg, C.D., 2013. Petrogenesis of Tertiary hornblendebearing lavas in the Rhön. Germany. J Petrol 54, 2095–2123.
Mayer, B., Jung, S., Romer, R.L., Pfänder, J.A., Klügel, A., Pack, A., Gröner, E., 2014. Amphibole in alkaline basalts from intraplate settings: implications for the petrogenesis of alkaline lavas from the metasomatised lithospheric mantle. Contrib. Mineral. Petrol. 167–989.
McKenzie, D.P., 1972. Active tectonics of the Mediterranean region. Geophys. J. R. Astron. Soc. Can. 30, 109–185.
McKenzie, D., Bickle, M., 1988. The volume and composition of melt generated by extension of the lithosphere. J Petrol. 29 (3), 625–679.
McKenzie, D.P., O'Nions, R.K., 1991. Partial melt distribution from inversion of rare earth element concentrations. J. Petrol. 32, 1021–1991.
McKenzie, D., O'Nions, R.K., 1995. The source regions of ocean island basalts. J. Petrol. 36, 133–159.
Nielson, J.E., Noller, J.S., 1987. Processes of mantle metasomatism; Constraints from observations of composite peridotite xenoliths. In: In: Morris, E.M., Pasteris, J.D. (Eds.), Mantle Metasomatism and Alkaline Magmatism 215. Geological Society of America, Special Papers, pp. 61–76.
Nielson, J.E., Wilshire, H.G., 1993. Magma transport and metasomatism in the mantle: a critical review of current geochemical models. Am. Mineral. 78, 1117–1134.
Nier, A.O., 1938. The Isotopic constitution of strontium, barium, bismuth, thallium and mercury. Phis. Rev. 54, 275–278.
Niu, Y., 2008. The origin of alkaline lavas. Science 320, 883–884.
Niu, Y., 2009. Some basic concepts and problems on the petrogenesis of intra-plate ocean island basalts. Chinese Sci. Bull. 54, 4148–4160.
Niu, Y., O'Hara, M.J., 2003. Origin of ocean island basalts: a new perspective from petrology, geochemistry, and mineral physics considerations. J. Geophys. Res. 108, 2209. https://doi.org/10.1029/2002JB002048.
O'Nions, R.K., Carter, S.R., Evensen, N.M., Hamilton, P.J., 1979. Geochemical and cosmochemical applications of Nd isotope analysis. Ann. Rev. Earth Planet. Sci. 7, 11–38.
O'Reilly, S.Y., Griffin, W.L., Ryan, C.G., 1991. Residence of trace elements in metasomatized spinel lherzolite xenoliths: a proton microprobe study. Contrib. Mineral. Petrol. 109, 98–113.
Parlak, O., Kozlu, H., Demirkol, C., Delaloye, M., 1997. Intracontinental plio-quaternary volcanism along the African-Anatolian plate boundary, southern Turkey. Ofioliti 22, 111–117.
Pearce, J.A., 1983. Role of the sub-continental lithosphere in magma genesis at active continental margins. In: Hawkesworth, C.J., Norry, M.J. (Eds.), Continental Basalts and Mantle Xenoliths. Shiva, Cheshire, UK, pp. 230–249.
Pilet, S., Hernandez, J., Sylvester, P., Poujol, M., 2005. The metasomatic alternative for ocean island basalt chemical heterogeneity. Earth Planet. Sci. Lett. 236, 148–166.
Pilet, S., Baker, M.B., Stolper, E.M., 2008. Metasomatized lithosphere and the origin of alkaline lavas. Science 320, 916–919.
Pilet, S., Ulmer, P., Villiger, S., 2010. Liquid line of descent of a basanitic liquid at 1.5 GPa: constraints on the formation of metasomatic veins. Contrib. Mineral. Petrol. 159, 621–643.
Pilet, S., Baker, M.B., Müntener, O., Stolper, E.M., 2011. Monte Carlo simulations of metasomatic enrichment in the lithosphere and implications for the source of alkaline basalts. J. Petrol. 52, 1415–1442.
Polat, A., Kerrich, R., Casey, J.F., 1997. Geochemistry of Quaternary basalts erupted along the east Anatolian and Dead Sea fault zones of southern Turkey: implications for mantle sources. Lithos 40, 55–68.
Powell, W., Zhang, M., O'Reilly, S.Y., Tiepolo, M., 2004. Mantle amphibole trace-element and isotopic signatures trace multiple metasomatic episodes in lithospheric mantle, western Victoria. Australia. Lithos 75, 141–171.
Prouteau, G., Scaillet, B., Pichavant, M., Maury, R., 2001. Evidence for mantle metasomatism by hydrous silicic melts derived from subducted oceanic crust. Nature 410, 197–200.
Prytulak, J., Elliott, T., 2007. TiO_2 enrichment in ocean island basalts. Earth Planet. Sci. Lett. 263, 388–403.
Rapp, R.P., Shimizu, N., Norman, M.D., Applegate, G.S., 1999. Reaction between slab-derived melts and peridotite in the mantle wedge: experimental constraints at 3.8 GPa. Chem. Geol. 160, 335–356.

Romer, R.L., Forster, H.-J., Breitkreuz, C., 2001. Intracontinental extensional magmatism with a subduction fingerprint: the late Carboniferous Halle Volcanıc Complex (Germany). Contrib. Mineral. Petrol. 141, 201–221.
Rosenbaum, J.M., 1993. Mantle phlogopite: a significant lead repository? Chem. Geol. 106, 475–483.
Şaroğlu, F., Emre, Ö., Kuşcu, İ., 1992. The East Anatolian Fault Zone of Turkey. *Annales Tectonicae,* Special Issue-Supplement 6, 99–125.
Şen, P.A., Temel, A., Gourgaud, A., 2004. Petrogenetic modeling of Quaternary post-collisional volcanism: a case study of central and eastern Anatolia. Geol. Mag. 141, 81–98.
Şengör, A.M.C., Yılmaz, Y., 1981. Tethyan evolution of Turkey: a plate tectonic approach. Tectonophysics 75, 181–241.
Shaw, D.M., 1970. Trace element fractionation during anataxis. Geochim. Cosmochim. Acta 34, 237–243.
Sobolev, A.V., Hofmann, A.W., Sobolev, S.V., Nikogosian, I.K., 2005. An olivine-free mantle source of Hawaiian shield basalts. Nature 434, 590–597.
Sobolev, A.V., Hofmann, A.W., Kuzmin, D.V., Yaxley, G.M., Arndt, N.T., Chung, S.-L., Danyushevsky, L.V., Elliott, T., Frey, F.A., Garcia, M.O., Gurenko, A.A., Kamenetsky, V.S., Kerr, A.C., Krivolutskaya, N.A., Matvienkov, V.V., Nikogosian, I.K., Rocholl, A., Sigurdsson, I.A., Sushchevskaya, N.M., Teklay, M., 2007. The amount of recycled crust in sources of mantle-derived melts. Science 316, 412–417.
Sobolev, S.V., Sobolev, A.V., Kuzmin, D.V., Krivolutskaya, N.A., Petrunin, A.G., Arndt, N.T., Radko, V.A., Vasiliev, Y.R., 2011. Linking mantle plumes, large igneous provinces and environmental catastrophes. Nature 477, 312–316.
Stracke, A., Bizimis, M., Salters, V.J.M., 2003. Recycling oceanic crust: quantitative constraints. Geochem. Geophys. Geosystems 4, 8003. https://doi.org/10.1029/2001GC000223.
Sun, S.S., McDonough, W.F., 1989. Chemical and isotopic systematics of oceanic basalts: implications for mantle composition and processes. In: In: Saunders, A.D., Norry, M.J. (Eds.), Magmatism in the Ocean Basins, vol 42. Geological Society of London, Special Publication, pp. 313–345.
Taylor, S.R., McLennan, S.M., 1985. The Continental Crust; Its Composition and Evolution; an Examination of the Geochemical Record Preserved in Sedimentary Rocks. Blackwell, Oxford, pp. 312.
Thirlwall, M.F., Upton, B.G.J., Jenkins, C., 1994. Interaction between continental lithosphere and the Iceland plume Sr-Nd-Pb isotope geochemistry of Tertiary basalts, NE Greenland. J. Petrol. 35, 839–879.
Turcotte, D.L., Emerman, S.H., 1983. Mechanisms of active and passive rifting. Tectonophysics 94 (1-4), 39–50.
Walker, G.P.L., 1973. Explosive volcanic eruptions a new classification scheme. Geol. Rundschau 62, 431–446.
Wass, S.Y., Rogers, N.W., 1980. Mantle metasomatism-precursor to continental alkaline volcanism. Geochim. Cosmochim. Acta 44, 1811–1823.
Weis, D., Kieffer, B., Maerschalk, C., Barling, J., de Jong, J., Williams, G.A., Hanano, D., Pretorius, W., Mattielli, N., Scoates, J.S., Goolaerts, A., Friedman, R.M., Mahoney, J.B., 2006. High-precision isotopic characterization of USGS reference materials by TIMS and MC-ICP-MS. Geochem. Geophys. Geosystems 7 (Q08006), 30.
White, W.M., 1985. Sources of oceanic basalts: radiogenic isotopic evidence. Geology 13, 115–118.
White, R., McKenzie, D., 1989. Magmatism at rift zones – the generation of volcanic continental margins and Flood Basalts. J. Geophys Res-Solid Earth Planets 94 (B6), 7685–7729.
Wilson, M., Downes, H., 1991. Tertiary-quaternary extension-related alkaline magmatism in western and Central Europe. J. Petrol. 32 (4), 811–849.
Witte, M., Jung, S., Pfander, J.A., Romer, R.L., Mayer, B., Garbe-Schenberg, D., 2017. OIB signatures in basin-related lithosphere-derived alkaline basalts from the Batain basin (Oman) - constraints from $^{40}Ar/^{39}Ar$ ages and Nd–Sr–Pb–Hf isotopes. Lithos (286–287), 109–124.
Witt-Eickschen, G., Seck, H.A., Reys, C., 1993. Multiple enrichment processes and their relationships in the subcrustal lithosphere beneath the Eifel (Germany). J. Petrol. 34, 1–22.
Witt-Eickschen, G., Kaminsky, W., Kramm, U., Harte, B., 1998. The nature of young vein metasomatism in the lithosphere of the West Eifel (Germany): geochemical and isotopic constraints from composite mantle xenoliths from the Meerfelder Maar. J. Petrol. 39, 155–185.
Yılmaz, Y., Gürpınar, O., Yiğitbaş, E., 1988. Tectonic evolution of the Miocene basins at the Amanos mountains and the Maraş region. Turkish Ass. Petroleum Geologists Bull. 1, 52–72.
Yurtmen, S., Rowbotham, G., İşler, F., Floyd, P., 2000. Petrogenesis of quaternary alkali volcanics, Ceyhan-Turkey. In: In: Bozkurt, E., Winchester, J.A., Piper, J.D.A. (Eds.), Tectonics and Magmatism of Turkey and the Surrounding Area, vol 173. Geological Society, Speical Publications, pp. 489–512.
Yürür, T., Chorowıcz, J., 1998. Recent volcanism, tectonics and plate kinematics near the junction of African, Arabian and Anatolian plates in the eastern Mediterranean. J. Volcanol. Geotherm. Res. 148, 1–15.
Zhang, J.-J., Zheng, Y.-F., Zhao, Z.-F., 2009. Geochemical evidence for interaction between oceanic crust and lithospheric mantle in the origin of Cenozoic continental basalts in east-central China. Lithos 110, 305–326.
Zindler, A.W., Hart, S.R., 1986. Chemical geodynamics. Annu. Rev. Earth Planet. Sci. 14, 493–571.
Zou, H., Zindler, A., 1996. Constraints on the degree of dynamic partial melting and source composition using concentration ratios in magmas. Geochimi. Cosmochim. Acta. 60, 711–717.